J|A|C|S ARTICLES

Published on Web 03/10/2010

Elucidation of Amyloid β-Protein Oligomerization Mechanisms: Discrete Molecular Dynamics Study

B. Urbanc,*,† M. Betnel,‡ L. Cruz,† G. Bitan,§,|| and D. B. Teplow§,||

Department of Physics, Drexel University, Philadelphia, Pennsylvania 19104, Department of Physics, Boston University, Boston, Massachusetts 02215, and Department of Neurology, David Geffen School of Medicine, and Molecular Biology Institute and Brain Research Institute, University of California, Los Angeles, California 90095-7334

Received November 12, 2009; E-mail: brigita@drexel.edu

Abstract: Oligomers of amyloid β-protein (Aβ) play a central role in the pathology of Alzheimer's disease. Of the two predominant Aβ alloforms, Aβ_{1-40} and Aβ_{1-42}, Aβ_{1-42} is more strongly implicated in the disease. We elucidated the structural characteristics of oligomers of Aβ_{1-40} and Aβ_{1-42} and their Arctic mutants, [E22G]Aβ_{1-40} and [E22G]Aβ_{1-42}. We simulated oligomer formation using discrete molecular dynamics (DMD) with a four-bead protein model, backbone hydrogen bonding, and residue-specific interactions due to effective hydropathy and charge. For all four peptides under study, we derived the characteristic oligomer size distributions that were in agreement with prior experimental findings. Unlike Aβ_{1-40}, Aβ_{1-42} had a high propensity to form paranuclei (pentameric or hexameric) structures that could self-associate into higher-order oligomers. Neither of the Arctic mutants formed higher-order oligomers, but [E22G]Aβ_{1-40} formed paranuclei with a similar propensity to that of Aβ_{1-42}. Whereas the best agreement with the experimental data was obtained when the charged residues were modeled as solely hydrophilic, further assembly from spherical oligomers into elongated protofibrils was induced by nonzero electrostatic interactions among the charged residues. Structural analysis revealed that the C-terminal region played a dominant role in Aβ_{1-42} oligomer formation whereas Aβ_{1-40} oligomerization was primarily driven by intermolecular interactions among the central hydrophobic regions. The N-terminal region A2-F4 played a prominent role in Aβ_{1-40} oligomerization but did not contribute to the oligomerization of Aβ_{1-42} or the Arctic mutants. The oligomer structure of both Arctic peptides resembled Aβ_{1-42} more than Aβ_{1-40}, consistent with their potentially more toxic nature.

Introduction

Alzheimer's disease (AD), characterized by the irreversible, progressive deterioration of learning and memory, is the dominant cause of dementia in the elderly. One of the hallmarks of AD is an accumulation of extracellular senile plaques, which contain fibrillar aggregates of the amyloid β-protein (Aβ). Genetic and experimental evidence strongly supports the hypothesis that low-order[1] oligomeric assemblies of Aβ, rather than fibrils, are the proximate neurotoxic agents in AD.[2−4] Aβ is produced through cleavage of the amyloid precursor protein (APP) and is normally present in the body predominantly in two alloforms, Aβ_{1-40} and Aβ_{1-42}, that differ structurally by the absence or presence of the two C-terminal amino acids Ile41-Ala42, respectively. Despite this relatively small difference in primary structure, Aβ_{1-42} oligomers are more toxic.[5] The proper targeting of therapeutic agents requires the elucidation of Aβ assembly dynamics and the determination of the site(s) responsible for imparting to Aβ_{1-42} its particular toxic potential. Different Aβ oligomeric assemblies may induce neurotoxicity by distinct mechanisms,[6] thus it is important to examine the oligomeric structure of specific order and under specific conditions when determining structure−toxicity correlations. A variety of oligomers have been reported to be toxic,[4] but none have been characterized structurally at the atomic level.

Aβ folding and assembly are remarkably complex processes, which complicates the application of classical structure determination methods such as X-ray crystallography and solution-state NMR to the oligomerization question.[7] A powerful approach providing information on the initial Aβ oligomerization process has been chemical cross-linking. The method of photoinduced cross-linking of unmodified proteins (PICUP), combined with SDS-PAGE, was used by Bitan et al. to

† Drexel University.
‡ Boston University.
§ Department of Neurology, David Geffen School of Medicine, University of California.
|| Molecular Biology Institute and Brain Research Institute, University of California.

(1) We note that "order" generally is used herein to define the number of Aβ monomers comprising a particular assembly. Unless stated otherwise, order does not refer to secondary or tertiary structure characteristics.

(2) Hardy, J.; Selkoe, D. J. *Science* **2002**, *297*, 353–356.
(3) Hardy, J. *Ann. Neurol.* **2003**, *54*, 143–144.
(4) Roychaudhuri, R.; Yang, M.; Hoshi, M. M.; Teplow, D. B. *J. Biol. Chem.* **2008**, *284*, 4749–53.
(5) Dahlgren, K. N.; Manelli, A. M.; Stine, W. B.; Baker, L. K.; Krafft, G. A.; LaDu, M. J. *J. Biol. Chem.* **2002**, *277*, 32046–32053.
(6) Deshpande, A.; Mina, E.; Glabe, C.; Busciglio, J. *J. Neurosci.* **2006**, *26*, 6011–6018.
(7) Teplow, D. B.; Lazo, N. D.; Bitan, G.; Bernstein, S.; Wyttenbach, T.; Bowers, M. T.; Baumketner, A.; Shea, J.-E.; Urbanc, B.; Cruz, L.; Borreguero, J.; Stanley, H. E. *Acc. Chem. Res.* **2006**, *39*, 635–645.

10.1021/ja9096303 © **2010 American Chemical Society**

determine the $A\beta_{1-40}$ and $A\beta_{1-42}$ oligomer size frequency distributions, revealing that the two alloforms form oligomers through distinct pathways.[8−10] $A\beta_{1-42}$ assembled into pentamer/hexamer units (paranuclei[11]) and multiples of paranuclei (dodecamers and octadecamers), but $A\beta_{1-40}$ formed only dimers, trimers, and tetramers that were in equilibrium with monomers. Recently, ion mobility spectrometry was applied to determine $A\beta_{1-40}$ and $A\beta_{1-42}$ oligomer distributions *in vitro* without the use of chemical cross-linking.[12] Bernstein et al. found distinct $A\beta_{1-40}$ and $A\beta_{1-42}$ oligomer distributions,[12] in agreement with PICUP/SDS-PAGE findings.[9] Oligomer size distributions have been found to be sensitive to single amino acid substitutions,[13] including those causing familial forms of AD and cerebral amyloid angiopathy. As such, the oligomer size distribution can be considered to be a "fingerprint" of a particular peptide and may be correlated with structural properties of the associated oligomers and protofibrils. However, neither PICUP/SDS-PAGE nor ion mobility spectrometry alone can directly reveal the interatomic interactions controlling the oligomerization process.

Molecular dynamics (MD) provides the means to visualize and quantify 3D atomic structures of proteins on timescales and in detail not possible experimentally. The number of computational approaches aimed at understanding $A\beta$ folding and assembly has increased substantially over the past decade. (See ref 14 for a review.) All-atom MD, which utilizes complete atomic models of $A\beta$, remains computationally untenable because of the large system size and simulation duration necessary to study $A\beta$ oligomerization.[7] For this reason, discrete molecular dynamics (DMD) combined with simplified protein models (one or two beads per residue) was explored to study protein folding.[15−21] However, these models require the native protein structure to be incorporated into interparticle interactions, which is undesirable for studies of natively disordered proteins such as $A\beta$. Intermediate-resolution models, such as the four-bead and united-atom models with backbone hydrogen bonding, which require knowledge only of the protein sequence, have been found to yield promising results when combined with DMD[22−26] or Monte Carlo dynamics.[27,28]

Recently, the DMD approach with either the four-bead protein model or a more sophisticated united-atom protein model (for a review, see ref 29) was applied to the $A\beta$ system. The results agreed with existing in vitro findings or were amenable to in vitro confirmation.[30−34] The DMD approach, which comprised the four-bead model, backbone hydrogen bonding, and the empirical hydropathy scale derived by Kyte and Doolittle,[35] demonstrated that the key differences in oligomerization between $A\beta_{1-40}$ and $A\beta_{1-42}$ resulted from the hydrophobic nature of the amino acids I41 and A42 present in $A\beta_{1-42}$,[31] in agreement with PICUP data.[13] When the effective electrostatic interaction among the charged amino acids was included in addition to the backbone hydrogen bonding and effective hydropathy, significantly larger oligomer sizes in both $A\beta_{1-40}$ and $A\beta_{1-42}$ were observed.[33] This is a particularly intriguing finding because more recent work on $A\beta_{1-40}$ and $A\beta_{1-42}$ folding showed that the electrostatic interaction did not affect folded structures in a significant way.[34] The oligomerization differences between the two alloforms were preceded by differences in the folded structures.[31,34] Specifically, $A\beta_{1-42}$ but not $A\beta_{1-40}$ was characterized by a turn structure centered at G37-G38, a prediction consistent with the findings of several independent experimental studies.[36−38] $A\beta_{1-42}$ and $A\beta_{1-40}$ folded structures also differed in the N-terminal region, where $A\beta_{1-40}$ but not $A\beta_{1-42}$ showed an increased β-strand propensity at A2-F4. The DMD approach was applied to examine temperature-induced changes in the secondary structure of the folded $A\beta_{1-40}$ and $A\beta_{1-42}$ as well as to characterize folding differences induced by Arctic mutation[39] E22G, which is associated with a familial form of AD characterized by an increased propensity for protofibril formation.[34] Interestingly, the E22G substitution induced structural differences in the N-terminal region, resulting in the folded

(8) Bitan, G.; Lomakin, A.; Teplow, D. B. *J. Biol. Chem.* **2001**, *276*, 35176–35184.
(9) Bitan, G.; Kirkitadze, M. D.; Lomakin, A.; Vollers, S. S.; Benedek, G. B.; Teplow, D. B. *Proc. Natl. Acad. Sci. U.S.A.* **2003**, *100*, 330–335.
(10) Bitan, G. *Methods Enzymol.* **2006**, *413*, 217–236.
(11) A paranucleus is defined by its secondary structure (∼18−24% β-sheet/β-turn and ∼3−7% α-helix), morphology (quasispherical by electron microscopy or atomic force microscopy), and quaternary structure (pentamer or hexamer).
(12) Bernstein, S. L.; Dupuis, N. F.; Lazo, N. D.; Wyttenbach, T.; Condron, M. M.; Bitan, G.; Teplow, D. B.; Shea, J.-E.; Ruotolo, B. T.; Robinson, C. V.; Bowers, M. T. *Nat. Chem.* **2009**, *1*, 326–331.
(13) Bitan, G.; Vollers, S. S.; Teplow, D. B. *J. Biol. Chem.* **2003**, *278*, 34882–34889.
(14) Urbanc, B.; Cruz, L.; Teplow, D. B.; Stanley, H. E. *Curr. Alzheimer Res.* **2006**, *3*, 493–504.
(15) Zhou, Y.; Hall, C. K.; Karplus, M. *Phys. Rev. Lett.* **1996**, *77*, 2822–2825.
(16) Smith, S. W.; Hall, C. K.; Freeman, B. D. *J. Comput. Phys.* **1997**, *134*, 16–30.
(17) Zhou, Y.; Karplus, M. *Proc. Natl. Acad. Sci. U.S.A.* **1997**, *94*, 14429–14432.
(18) Zhou, Y.; Karplus, M.; Wichert, J. M.; Hall, C. K. *J. Chem. Phys.* **1997**, *107*, 10691–10708.
(19) Dokholyan, N. V.; Buldyrev, S. V.; Stanley, H. E.; Shakhnovich, E. I. *Fold. Des.* **1998**, *3*, 577–587.
(20) Zhou, Y.; Karplus, M. *J. Mol. Biol.* **1999**, *293*, 917–951.
(21) Dokholyan, N. V.; Buldyrev, S. V.; Stanley, H. E.; Shakhnovich, E. I. *J. Mol. Biol.* **2000**, *296*, 1183–1188.
(22) Smith, A. V.; Hall, C. K. *J. Mol. Biol.* **2001**, *312*, 187–202.
(23) Smith, A. V.; Hall, C. K. *Proteins: Struct., Funct., Genet.* **2001**, *44*, 344–360.
(24) Smith, A. V.; Hall, C. K. *Proteins: Struct., Funct., Genet.* **2001**, *44*, 376–391.
(25) Ding, F.; Borreguero, J. M.; Buldyrev, S. V.; Stanley, H. E.; Dokholyan, N. V. *Proteins: Struct., Funct., Genet.* **2003**, *53*, 220–228.
(26) Ding, F.; Buldyrev, S. V.; Dokholyan, N. V. *Biophys. J.* **2005**, *88*, 147–155.
(27) Fitzgerald, J. E.; Jha, A. K.; Colubri, A.; Sosnick, T. R.; Freed, K. F. *Protein Sci.* **2007**, *16*, 2123–2139.
(28) DeBartolo, J.; Colubri, A.; Jha, A.; Fitzgerald, J. E.; Freed, K. F.; Sosnick, T. R. *Proc. Natl. Acad. Sci. U.S.A.* **2009**, *106*, 3734−3739.
(29) Urbanc, B.; Borreguero, J. M.; Cruz, L.; Stanley, H. E. *Methods Enzymol.* **2006**, *412*, 314–338.
(30) Urbanc, B.; Cruz, L.; Ding, F.; Sammond, D.; Khare, S.; Buldyrev, S. V.; Stanley, H. E.; Dokholyan, N. V. *Biophys. J.* **2004**, *87*, 2310–2321.
(31) Urbanc, B.; Cruz, L.; Yun, S.; Buldyrev, S. V.; Bitan, G.; Teplow, D. B.; Stanley, H. E. *Proc. Natl. Acad. Sci. U.S.A.* **2004**, *101*, 17345–17350.
(32) Borreguero, J. M.; Urbanc, B.; Lazo, N. D.; Buldyrev, S. V.; Teplow, D. B.; Stanley, H. E. *Proc. Natl. Acad. Sci. U.S.A.* **2005**, *102*, 6015–6020.
(33) Yun, S.; Urbanc, B.; Cruz, L.; Bitan, G.; Teplow, D. B.; Stanley, H. E. *Biophys. J.* **2007**, *92*, 4064–4077.
(34) Lam, A.; Teplow, D. B.; Stanley, H. E.; Urbanc, B. *J. Am. Chem. Soc.* **2008**, *130*, 17413–17422.
(35) Kyte, J.; Doolittle, R. F. *J. Mol. Biol.* **1982**, *157*, 105–132.
(36) Lazo, N. D.; Grant, M. A.; Condron, M. C.; Rigby, A. C.; Teplow, D. B. *Protein Sci.* **2005**, *14*, 1581–1596.
(37) Murakami, K.; Irie, K.; Ohigashi, H.; Hara, H.; Nagao, M.; Shimizu, T.; Shirasawa, T. *J. Am. Chem. Soc.* **2005**, *127*, 15168–15174.
(38) Yan, Y.; Wang, C. *J. Mol. Biol.* **2006**, *364*, 853–862.
(39) Nilsberth, C.; Westlind-Danielsson, A.; Eckman, C. B.; Condron, M. M.; Axelman, K.; Forsell, C.; Stenh, C.; Luthman, J.; Teplow, D. B.; Younkin, S. G.; Naslund, J.; Lannfelt, L. *Nat. Neurosci.* **2001**, *4*, 887–893.

structures of both the Aβ_{1-40} and Aβ_{1-42} Arctic mutants showing a greater resemblance to wild-type (WT) Aβ_{1-42}.[34]

In this work, we applied the *ab initio* DMD approach with two implicit solvent parameters to examine the early events in assembly pathways of Aβ_{1-40}, Aβ_{1-42}, [E22G]Aβ_{1-40}, and [E22G]Aβ_{1-42}. Adjusting the two solvent parameters to replicate experimental solvent conditions is important because Aβ folding and assembly strongly depend on the solvent.[40−42] Earlier applications of the DMD approach to Aβ folding and oligomer formation[30,31,33,34] and subsequent comparison of the results to *in vitro* PICUP data on oligomer size distributions[9,13] and to the average amounts of β-strand in monomeric and oligomeric states[43,44] showed consistent agreement between computational and experimental results for the same narrow range of the two implicit solvent parameters. The present work builds upon the assumptions that the oligomer size distributions are correctly represented by an experimental technique using PICUP/SDS-PAGE and that our DMD approach captures the key features relevant to folding, early assembly pathways, and the resulting structures of the four Aβ peptides under study. Here, relative to our earlier study,[31] we simulated Aβ_{1-40} and Aβ_{1-42} oligomerization for twice as many time steps (20×10^6), extended the main production runs to 40×10^6, and incorporated a more accurate estimate of the physiological temperature, changes that allowed us to obtain closer agreement with experimentally derived oligomer size distributions.[9] Using these changed simulation parameters, we then examined the role of weak electrostatic interactions between charged amino acids in the formation of both quasispherical oligomers and the more elongated protofibril-like assemblies into which they convert. Finally, we applied the DMD simulations with the same implicit solvent parameters and followed the same simulation protocol as for the WT peptides to examine the effects of the Arctic mutation on the oligomerization pathways and structural properties of the resulting oligomers.

Methods

The advantages and limitations of the DMD approach with the four-bead protein model, backbone hydrogen bonding, and amino acid-specific interactions modeling the solvent implicitly were described in detail in ref 29. Below, we briefly summarize key characteristics of this computational approach.

Discrete Molecular Dynamics. MD can be reduced to discrete molecular dynamics (DMD) whenever the interparticle potentials are approximated by a single square well or a combination of square wells.[45] DMD is event-driven, and each event corresponds to a collision between a pair of particles. Particles move along straight lines at constant speeds between two succeeding collisions. Instead of integrating Newton's equations at every time step for every particle to obtain a complete trajectory, DMD requires only an efficient sorting of the collision times between pairs of particles and the selection of the shortest one, which determines the time of the next event/collision. Consequently, DMD is orders of magnitude faster than MD. In our DMD approach,[29] the simulation volume and number of particles are fixed, the temperature is held constant by the Berendsen thermostat,[46] and periodic boundary conditions are implemented.

In contrast to all-atom MD in explicit solvent, in which an explicit time step (e.g., 1 ps) ensures a direct comparison between simulation and experimental timescales, event-driven DMD with implicit solvent lacks such an "absolute" timescale because the collisions between the protein atoms and solvent and those among solvent atoms are not explicitly modeled. Consequently, the relationship between the DMD simulation and real time may not be a simple linear function. Thus, a direct comparison of the DMD-derived kinetics of protein folding and assembly to experimentally obtained data is not straightforward. However, DMD is dynamics in a true sense in that it results in a causally related sequence of events. In our study, the sequence of events includes all stages of folding from unstructured, random coil-like monomers, followed by assembly into oligomers and potentially larger aggregates.

Four-Bead Protein Model with Backbone Hydrogen Bonding. In the four-bead protein model, the backbone is represented by three beads corresponding to the amide (N), the α-carbon (C_α), and the carbonyl (C) groups. Each side chain, except glycine, is represented by one side-chain bead (C_β). Four beads per amino acid is the smallest number of beads that can capture the chiral nature of an individual amino acid (i.e., a lack of mirror symmetry in all amino acids except glycine). The lengths of bonds and the angular constraints are determined phenomenologically by calculating their distributions using the known folded protein structures of ∼7700 proteins from the Protein Data Bank (PDB).[47] The values of the lengths of covalent bonds and the angular constraints are allowed to fluctuate around their average values with the fluctuation amplitude set to 2% of the average value.[25] The effective backbone hydrogen bond is implemented between the nitrogen atom N_i of the *i*th amino acid and the carbon atom C_j of the *j*th amino acid.[25] For the hydrogen bond to form, the neighboring backbone atoms need to be at correct distances from the atoms involved in hydrogen bond formation to account for the anisotropic character of the hydrogen bond. The strength of the backbone hydrogen bond interaction, E_{HB}, represents a unit of energy, and the temperature is given in units of E_{HB}/k_B.

Amino Acid-Specific Interactions Due to Hydropathy and Charge. To account implicitly for the aqueous solvent, we previously implemented the effective amino acid-specific hydropathic interactions between the C_β atoms[31] using the hydropathy scale derived by Kyte and Doolittle.[35] At neutral pH, amino acids I, V, L, F, C, M, and A were considered to be hydrophobic, N, Q, and H were considered to be noncharged hydrophilic, and R, K, D, and E were considered to be charged hydrophilic. The remaining amino acids with absolute values of hydropathies below threshold values were treated as neutral. Only $C_\beta-C_\beta$ interactions within the group of hydrophobic residues and within the group of hydrophilic residues were allowed. The rest of the $C_\beta-C_\beta$ interactions were due to only the excluded volume (hard sphere) repulsion. Each C_β atom was associated with a hydropathy parameter normalized between −1 (for the most hydrophobic residue) to +1 (for the most hydrophilic residue). The effective hydropathic interaction was modeled by a single square-well potential with the absolute value of the potential energy (or the strength of the interaction) equal to E_{HP} and an interaction range of 0.75 nm. When the $C_\beta-C_\beta$ distance of two hydrophobic/hydrophilic side-chain atoms decreased from above to below 0.75 nm (but remained larger than the sum of their hard-sphere radii), they experienced an attractive/repulsive interaction equal to E_{HP} multiplied by the average of their respective hydropathy parameters. The implicit solvent parameter E_{HP}, which

(40) Zhang, S.; Iwata, K.; Lachenmann, M. J.; Peng, J. W.; Li, S.; Stimson, E. R.; Lu, Y.; Felix, A. M.; Maggio, J. E.; Lee, J. P. *J. Struct. Biol.* **2000**, *130*, 130–141.
(41) Crescenzi, O.; Tomaselli, S.; Guerrini, R.; Salvadori, S.; D'Ursi, A. M.; Temussi, P. A.; Picone, D. *Eur. J. Biochem.* **2002**, *269*, 5642–5648.
(42) Fezoui, Y.; Teplow, D. B. *J. Biol. Chem.* **2002**, *277*, 36948–36954.
(43) Kirkitadze, M. D.; Condron, M. M.; Teplow, D. B. *J. Mol. Biol.* **2001**, *312*, 1103–1119.
(44) Lim, K. H.; Collver, H. H.; Le, Y. T.; Nagchowdhuri, P.; Kenney, J. M. *Biochem. Biophys. Res. Commun.* **2007**, *353*, 443–449.
(45) Rapaport, D. C. *The Art of Molecular Dynamics Simulation*; Cambridge University Press: Cambridge, U.K., 1997.
(46) Berendsen, H. J. C.; Postma, J. P. M.; van Gunsteren, W. F.; DiNola, A.; Haak, J. R. *J. Chem. Phys.* **1984**, *8*, 3684–3690.
(47) Berman, H. M.; Westbrook, J.; Feng, Z.; Gilliland, G.; Bhat, T. N.; Weissig, H.; Shindyalov, I. N.; Bourne, P. E. *Nucleic Acids Res.* **2000**, *28*, 235–242.

strongly depends on the presence or absence of water in the solvent, was set to $E_{HP} = 0.3$ (in units of E_{HB}) as in the previous study.[31] The interaction between two hydrophobic side chains was attractive to model the tendency of each hydrophobic residue to decrease its solvent exposure. The interaction between two hydrophilic side chains was repulsive to model the tendency of each hydrophilic residue to maximize its solvent exposure. The implementation of the effective electrostatic interaction between charged residues is given below. Note that in the absence ($E_{CH} = 0$) of the effective electrostatic interaction between the charged hydrophilic residues, two C_β atoms of the same or of the opposite charge experience effective hydrophilic repulsion. This state corresponds to solvent conditions in which all charged groups are completely screened by solvent water molecules, disabling electrostatic interactions among them.

The effective electrostatic interaction between two charged side-chain atoms was implemented using a double attractive/repulsive square well potential and an interaction range of 0.75 nm.[29] The absolute value of the potential energy associated with the electrostatic interaction was E_{CH} (in units of E_{HB}), which was experienced between two charged C_β atoms at a distance <0.6 nm (the soft interaction range). Here we used very small strengths of the effective electrostatic interactions, $E_{CH} = 10^{-6}$ or 10^{-2} (in units of E_{HB}). In contrast to the case of $E_{CH} = 0$ in which the charged amino acids R, K, D, and E were considered to be purely hydrophilic, when $E_{CH} = 10^{-6}$ or 10^{-2} the charged amino acids interacted among themselves through their electrostatic but not their hydrophilic properties, even though the corresponding strengths of the electrostatic interaction were small compared to E_{HB}. Note that even with $E_{CH} > 0$ there was an effective hydrophilic repulsion between two noncharged hydrophilic C_β atoms as well as between a charged and a noncharged hydrophilic C_β atom. The implicit solvent parameter values $E_{CH} = 10^{-6}$ and 10^{-2} would correspond to the solvent conditions under which the charged groups were only partially screened by solvent water.

Simulation Conditions. The primary structure of $A\beta_{1-42}$ is ^{1}DAEFRHDSGY ^{11}EVHHQKLVFF ^{21}AEDVGSNKGA ^{31}IIGLMVGGVV ^{41}IA.

The shorter alloform, $A\beta_{1-40}$, lacks the C-terminal amino acids $I_{41}A_{42}$. Following the previous notation,[31,33,34] we will refer to the region L17-A21 as the central hydrophobic cluster (CHC), the region I31-V36 as the midhydrophobic region (MHR), and the region V39-V40/A42 as the C-terminal region (CTR).

Previously, we demonstrated that the four-bead DMD approach was successful in capturing oligomer size distribution differences between $A\beta_{1-40}$ and $A\beta_{1-42}$. $A\beta_{1-40}$ produced an oligomer size distribution with a high dimer frequency and decreasing numbers of higher-order oligomers, whereas $A\beta_{1-42}$ displayed a pentamer peak in addition to a dimer peak.[31] Although these simulation results were consistent with experimentally observed oligomer frequency distributions,[9] they did not yield significant numbers of $A\beta_{1-42}$ hexamers or oligomers with orders of 10−12 that were found experimentally. To address this issue, we have extended the simulation times and employed a more physiological temperature, $T = 0.13$ (in units of E_{HB}/k_B) versus 0.15 used previously. Longer simulation times were employed because oligomeric states are metastable and are hypothesized eventually to evolve through protofibrils to fibril states. $T = 0.13$ was chosen because recent simulations of $A\beta_{1-40}$ and $A\beta_{1-42}$ folding[34] have shown that when $T \in (0.12, 0.13)$, the population-average β-strand ($\langle\beta\text{-strand}\rangle$) content most accurately represents that found experimentally.[44]

We simulated oligomer formation starting from 32 spatially separated noninteracting and unfolded $A\beta$ peptides in a cubic box of 25 nm. Initial distinct populations of conformers for eight trajectories of each alloform were obtained by performing short, high-temperature ($T = 4$) DMD simulation runs and saving configurations every 0.1×10^6 simulation steps. Eight production runs each for $A\beta_{1-40}$ and $A\beta_{1-42}$ then were performed for 20×10^6 and for the optimal implicit solvent parameters further extended to 40×10^6 simulation steps.

Table 1. Total Number of Conformers from Monomers ($n = 1$) to Oligomers of Order $n = 2-6$ Used in the Structural Analysis[a]

number of conformers	$n = 1$	$n = 2$	$n = 3$	$n = 4$	$n = 5$	$n = 6$
$A\beta_{1-40}$	108	396	336	110	12	24
$A\beta_{1-42}$	56	215	177	54	56	59
[E22G] $A\beta_{1-40}$	61	266	189	83	70	69
[E22G] $A\beta_{1-42}$	69	129	230	144	57	43

[a] The conformers were obtained using 8 trajectories per peptide and 11 time frames between 19×10^6 and 20×10^6 time steps per trajectory.

Table 2. Average Amounts of the β-Strand Propensity in $A\beta_{1-40}$ and $A\beta_{1-42}$ at Simulation Times between 19×10^6 and 20×10^6 Steps for Three Different Interaction Schemes[a]

$\langle\beta\text{-strand}\rangle$	$A\beta_{1-40}$ (%)	$A\beta_{1-42}$ (%)
$E_{CH} = 0$	17.2 ± 1.5	18.6 ± 1.5
$E_{CH} = 10^{-6}$	16.9 ± 1.5	19.1 ± 1.6
$E_{CH} = 0.01$	18.6 ± 1.6	20.6 ± 1.6

[a] The error bars correspond to SEM.

Structural Analysis. Quasispherical oligomers formed by $A\beta_{1-40}$ and $A\beta_{1-42}$, from dimers through pentamers, were structurally characterized in the previous study.[31] The structures of $A\beta_{1-40}$ and $A\beta_{1-42}$ trimers and tetramers showed structural characteristics that partially overlapped with those of dimers and pentamers, suggesting a monotonic structural evolution from dimers through pentamers.

In the present study, 8 trajectories of 32 peptides each were produced for the 4 peptides under study. In the oligomer size distribution calculation, we considered realizations for time frames of 19×10^6, 19.5×10^6, and 20×10^6 simulation steps to facilitate the comparison of the current and previous work.[31] For the rest of the analyses, realizations at 11 time frames of between 19×10^6 and 20×10^6 simulation steps (at 10^5-step intervals) were considered. Each realization consisted of a mixture of monomers as well as oligomers of various order. A criterion used to determine whether two peptide chains, A and B, belonged to the same oligomer was based on the threshold distance of 0.75 nm between the centers of mass of an atom of chain A and an atom of chain B. If any pair of such atoms was at a distance smaller than 0.75 nm, chains A and B were assigned to the same oligomer.

Prior to the analysis, PDB[47] files of individual monomers and oligomers were extracted from all realizations and sorted by oligomer order. Oligomers of a particular order that were most abundantly represented in the probability distribution of oligomer sizes were, by definition, those with the lowest free energies. In our structural analysis, we thus selected dimers and hexamers that were relatively abundant in all peptides. We did so because the corresponding oligomer structures were representative, which was needed to highlight the differences among the four peptides, and the number of actual oligomer conformations[48] was large enough to produce statistically reliable results. In addition, dimer formation is the first step in oligomerization, thus it is important to compare structurally dimers of the four peptides under study and hexamers, which are hypothesized to be among the most toxic $A\beta_{1-42}$ oligomers. In total, across 8 different trajectories and 11 time frames per peptide, there were 396 $A\beta_{1-40}$, 215 $A\beta_{1-42}$, 266 [E22G]$A\beta_{1-40}$, and 129 [E22G]$A\beta_{1-42}$ dimers and 24 $A\beta_{1-40}$, 59 $A\beta_{1-42}$, 69 [E22G]$A\beta_{1-40}$, and 43 [E22G]$A\beta_{1-42}$ hexamers, yielding a set of conformers large enough to power statistical analyses of the structural data (Table 1).

Oligomer Size Distribution. Because oligomer size distributions evolved with time, we selected for the calculation of probability

(48) We use the term oligomer conformation to refer to a collection of all spatial coordinates of all atoms of all peptide chains comprising a single oligomer.

distributions a relatively narrow time window of 1×10^6 steps, within which the distributions did not change significantly. Within this window, we selected three time frames such that the corresponding populations of monomers and oligomers were as independent of each other as possible to avoid biasing the averaging and standard error calculations. Thus, for each peptide, 24 distinct realizations from 8 trajectories (each comprising 32 peptides) for time frames of 19×10^6, 19.5×10^6, and 20×10^6 steps were analyzed. For each of these 24 realizations per peptide, the probability distributions of monomers and oligomers of all sizes were calculated. The final normalized probability distributions of monomers and oligomers of all orders and the standard errors of the mean (SEM) were calculated as averages over 24 individual probability distributions. All oligomer size distributions reported in this work were calculated using the same protocol. To address the concern of 24 not being a sufficient number of frames, we also recalculated all of the size distributions by considering 11 time frames (from 19 million to 20 million time steps, taking into account conformations 100 000 steps apart) instead of 3 time frames (at 19 million, 19.5 million, and 20 million time steps)—in total 88 frames (instead of 24). The resulting size distributions were smoother but essentially overlapping within the SEM values with the original distributions (data not shown).

Secondary Structure. Amino acid-specific propensities for secondary structure formation were calculated using the STRIDE program[49,50] within the Visual Molecular Dynamics (VMD) software package.[51] The secondary structure propensities included several types of α-helical, β-strand, turn, and bridge structures. Here we analyzed in detail the dominant secondary structure elements, β-strand and turn.

Solvent-Accessible Surface Area (SASA). We calculated the solvent-accessible surface area per amino acid (SASA) by using VMD.[51] In addition to the four atoms per amino acid (three for glycine), we also considered the backbone carbonyl oxygen and amide hydrogen involved in hydrogen bond formation. This calculation created a spherical surface around each atom in the amino acid, 1.4 Å away from the atom's van der Waals surface, resulting in a combined 3D surface around each amino acid. SASA was then defined by calculating the part of this surface area that did not overlap with any other surface belonging to the neighboring amino acids and was thus accessible to the implicit solvent. Amino acids that were buried inside an assembly had a smaller SASA whereas amino acids on the surface assumed a higher SASA.

Contact Maps with Hydrogen Bond Propensities. By definition, two amino acids were deemed to be in contact if the distance between their centers of mass was ≤ 0.75 nm. The contact map was defined as a matrix in which the value of each (i, j) element was equal to an average number of contacts between amino acids i and j. We distinguished intra- and intermolecular contact maps. If amino acids i and j belonged to the same peptide, then the corresponding contacts contributed to the intramolecular contact map. If not, the contacts contributed to the intermolecular contact map. The contact map of each assembly was normalized by the number of contributing peptide molecules and by the maximal number of contacts between two residues. Because of the four-bead representation, the maximal number of intramolecular contacts was $4^2 = 16$. Consequently, the average number of intramolecular contacts between residues i and j normalized by a factor of 16 could not surpass 1. After normalizing the intermolecular contact map in the same way, the maximal number of contacts between residues i and j could be larger than 1 because amino acid i of one molecule could be surrounded by several amino acids j belonging to different molecules.

The contact map described above did not distinguish between the types of interactions between the two amino acids in contact. The contact between two amino acids could be due to the effective hydrophobic attraction, attractive electrostatic interaction, backbone hydrogen bonding, or simply the proximity to neighboring amino acids involved in an attractive interaction. Because backbone hydrogen bonding is key to secondary structure formation, we focused specifically on amino acids involved in backbone hydrogen bond formation. We defined intra- and intermolecular hydrogen bond maps for each pair of amino acids as an average number of backbone hydrogen bonds between the two amino acids. The pairs of amino acids involved in backbone hydrogen bond formation were identified within each oligomer conformation (PDB file) using VMD. Depending on whether the amino acids belonged to the same or to different peptide chains, these pairs contributed to either intra- or intermolecular hydrogen bond maps. Each amino acid (except proline) can form up to two intermolecular backbone hydrogen bonds, as, for example, inside a β-sheet structure. Consequently, both intra- and intermolecular hydrogen bond map values can assume any value between 0 and 2. The final contact maps with average numbers of intra- and intermolecular hydrogen bonds were then obtained by averaging the individual hydrogen bond maps over all oligomer conformations (PDB files) of specific oligomer order.

Relative Distance per Residue. By inspection, oligomers (dimers through hexamers) of the four peptides under study were quasispherical. To gain information on an average oligomer size and an average arrangement of individual residues within the oligomer with respect to its center of mass, we calculated the average relative distance from the center of mass per residue as in the prior work.[31] For each oligomer, we first computed the center of mass and the distances of C_α atoms of individual residues from the center of mass. We separately calculated the averages over all dimers and all hexamers for all four peptides, resulting in eight different curves of the average relative distance per residue. We then could identify the peptide regions that were (i) most distant from the center of mass and thus determine the average diameters of dimers and hexamers (the distance between the most distant C_α atom from the center of mass was defined as one-half of an average oligomer diameter) and (ii) closest to the center of mass. If these latter minimal relative distances (ii) were considerably larger than ~0.5 nm, then this result would indicate that the shape of oligomers was more ellipsoidal than spherical, providing insight into their shape as well as the structure and assembly.[52] In this case, the estimation of the oligomer size as defined by (i) would correspond to the largest diameter of the ellipsoidally shaped oligomer.

Results

Initial conditions for our simulations included 32 noninteracting monomeric peptides per trajectory. These peptides were spatially separated, and in the early stages of all production runs, folding occurred prior to assembly into oligomers. Our initial study reported the sequence of folding events in $A\beta_{1-40}$ and $A\beta_{1-42}$, quantified the differences between $A\beta_{1-40}$ and $A\beta_{1-42}$ folded structures,[31] and was followed by a systematic study of monomer folding in $A\beta_{1-40}$ and $A\beta_{1-42}$ and their Arctic mutants.[34] We focus here on the formation of oligomeric assemblies in $A\beta_{1-40}$, $A\beta_{1-42}$, [E22G]$A\beta_{1-40}$, and [E22G]$A\beta_{1-42}$.

Our DMD approach is based on two implicit solvent parameters, E_{HP} and E_{CH}, which need to be adjusted to the specific solvent under study. Lam *et al.* used the DMD approach to study the temperature dependence of the average β-strand in $A\beta_{1-40}$ and $A\beta_{1-42}$ folded monomers and demonstrated that the average amount of β-strand in folded monomers critically

(49) Frishman, D.; Argos, P. *Proteins: Struct., Funct., Genet.* **1995**, *23*, 566–579.
(50) Heinig, M.; Frishman, D. *Nucleic Acids Res.* **2004**, *32*, W500–502.
(51) Humphrey, W.; Dalke, A.; Schulten, K. *J. Mol. Graph.* **1996**, *14*, 33–38.

(52) An ellipsoidal shape of an oligomer of the nth order would indicate that the oligomer was formed by merging two spherical oligomers of orders n_1 and n_2, $n = n_1 + n_2$.

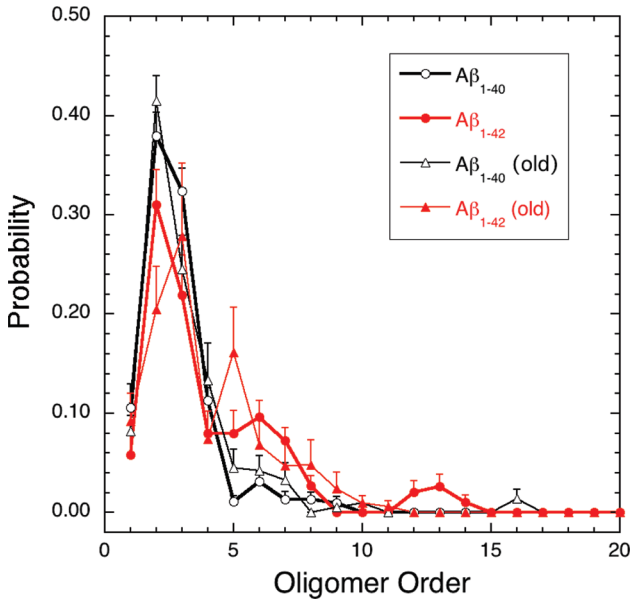

Figure 1. Oligomer size distributions for $A\beta_{1-40}$ (black curve) and $A\beta_{1-42}$ (red curve) obtained *in silico* using DMD with the four-bead protein model at $T = 0.130$. Each distribution is an average over eight 20×10^6 simulation steps long trajectories. All conformations for time frames at 19×10^6, 19.5×10^6, and 20×10^6 simulation steps were included in the analysis. Each trajectory involved 32 peptides, initially spatially separated and each in a random coil conformation enclosed in a 25-nm-length cubic box. The error bars represent SEM. For comparison, old simulation data reported by Urbanc *et al.*[31] for $A\beta_{1-40}$ (thin black curve) and $A\beta_{1-42}$ (thin red curve), obtained at $T = 0.150$ by averaging over eight 10×10^6 simulation steps long trajectories, are shown.

depends on E_{HP} (and not strongly on E_{CH}) and that the range of E_{HP} that matches experimental circular dichroism intensities[44] best is $E_{HP} \in [0.3, 0.4]$,[34] also in agreement with our earlier oligomerization study.[31] This comparison of the β-strand values obtained *in silico* and *in vitro* also resulted in an estimate of physiological temperature, 0.12−0.13 (in units of E_{HB}/k_B).[34] In the present study, we showed that by setting the two implicit solvent parameters $E_{HP} = 0.3$ and $E_{CH} = 0$ and using $T = 0.13$ for the physiological temperature, a simultaneous match of both $A\beta_{1-40}$ and $A\beta_{1-42}$ oligomer size distributions to the experimental values was obtained. Then, we applied the same DMD simulation protocol with the same implicit solvent parameters and physiological temperature to conduct the DMD simulations of two Arctic mutants to obtain [E22G]$A\beta_{1-40}$ or [E22G]$A\beta_{1-42}$ oligomer size distributions, which were experimentally shown to differ significantly from each other as well as from the distributions of the WT peptides.[13]

The results of the present study are organized as follows. First, probability distributions of $A\beta_{1-40}$ and $A\beta_{1-42}$ conformers obtained by our DMD approach are analyzed and compared to the results of our earlier study.[31] Second, the role of effective electrostatic interactions in $A\beta_{1-40}$ and $A\beta_{1-42}$ assembly is studied. Third, using the same simulation parameters, probability distributions of [E22G]$A\beta_{1-40}$ and [E22G]$A\beta_{1-42}$ are derived and compared to *in vitro* PICUP data.[13] Fourth, dimer and hexamer structures of all four peptides are characterized by calculating the β-strand and turn propensities, SASA per residue, and contact maps. Finally, the formation of higher-order oligomers is addressed.

Oligomer Size Distribution of Wild-Type Aβ. We found that the $A\beta_{1-40}$ oligomer size distribution was not significantly different (Figure 1, thick black curve) from the one obtained in our previous work (Figure 1, thin black curve).[31] The new distribution for $A\beta_{1-40}$ showed a slightly increased frequency of trimers and decreased frequencies of pentamers and hexamers. The $A\beta_{1-42}$ oligomer size distribution, however, showed a significant number of hexamers as well as an additional peak at the dodecamer/tridecamer (Figure 1, thick red curve) that was not present in the previous simulations (Figure 1, thin red curve).[31] Doubling the simulation time (from 10×10^6 to 20×10^6) and using a more physiologic temperature estimate ($T = 0.13$ instead of $T = 0.15$) thus produced distributions that were more realistic as determined by comparison with the *in vitro* oligomer size distributions obtained by PICUP.[9]

Role of Effective Electrostatic Interactions in Aβ Oligomerization. The results described above were obtained by using the same implicit solvent parameters, $E_{HP} = 0.3$ and $E_{CH} = 0$, as used previously, where all charged amino acids were treated as solely polar with no electrostatic charge.[31] The reasoning behind this interaction scheme was an assumption that the charged amino acid side-chain groups are completely screened by surrounding water molecules in this early stage of assembly. In contrast to this assumption, substantial experimental evidence indicates that the D23-K28 salt bridge plays an important role in the fibril formation of the WT peptides grown under agitated conditions.[53−56] E22-K28 and D23-K28 salt bridges also were shown to stabilize a turn in the A21-A30 peptide segment that evidence suggests nucleates the folding of full-length Aβ.[32,36,57,58]

A prior DMD study on the effect of electrostatic interactions on $A\beta_{1-40}$ and $A\beta_{1-42}$ oligomer formation demonstrated that an effective electrostatic interaction potential energy of $E_{CH} = 0.6$ promoted higher-order oligomer formation for both alloforms. The oligomer sizes were considerably larger than the sizes measured experimentally.[33] This result could be due to the fact that in an aqueous solution water molecules interact with charged hydrophilic residues and thereby effectively screen the electrostatic interactions between pairs of charged residues. Consequently, the potential energy of effective electrostatic interactions of $E_{CH} = 0.6$ in the study of Yun *et al.* would be overestimated.[33] However, a recent DMD study showed that $A\beta_{1-40}$ and $A\beta_{1-42}$ folding was almost unaltered over a wide temperature range for effective electrostatic interaction strengths of $E_{CH} \leq 0.3$.[34] It is thus important to address the question of whether subtle changes in the interaction between charged amino acids affect the oligomer size distribution.

To answer the question posed above, we studied three different cases: $E_{CH} = 0$, 10^{-6}, and 10^{-2}. The difference between the cases of $E_{CH} = 0$ and 10^{-6} was in the way that the charged amino acids interacted among themselves. In the former case, a pair of charged amino acids experienced effective hydrophilic repulsion independent of the respective charges, and in the later case, a pair of charged amino acids experienced a small effective electrostatic attraction or repulsion, depending on their respective

(53) Petkova, A. T.; Leapman, R. D.; Guo, Z.; Yau, W.-M.; Mattson, M. P.; Tycko, R. *Science* **2005**, *307*, 262–265.
(54) Luhrs, T.; Ritter, C.; Adrian, M.; Riek-Loher, D.; Bohrmann, B.; Dobeli, H.; Schubert, D.; Riek, R. *Proc. Natl. Acad. Sci. U.S.A.* **2005**, *102*, 17342–17347.
(55) Sciarretta, K. L.; Gordon, D. J.; Petkova, A. T.; Tycko, R.; Meredith, S. C. *Biochemistry* **2005**, *44*, 6003–6014.
(56) Petkova, A. T.; Yau, W.-M.; Tycko, R. *Biochemistry* **2006**, *45*, 498–512.
(57) Cruz, L.; Urbanc, B.; Borreguero, J. M.; Lazo, N. D.; Teplow, D. B.; Stanley, H. E. *Proc. Natl. Acad. Sci. U.S.A.* **2005**, *102*, 18258–18263.
(58) Grant, M. A.; Lazo, N. D.; Lomakin, A.; Condron, M. M.; Arai, H.; Yamin, G.; Rigby, A. C.; Teplow, D. B. *Proc. Natl. Acad. Sci. U.S.A.* **2007**, *104*, 16522–16527.

charges, but no effective hydrophilic repulsion. Because the potential energy associated with the later case was small (10^{-6}) compared to the thermal energy ($k_BT = 0.13$), charged amino acids effectively interacted only through repulsive hard-sphere excluded volume interactions. In the third case, $E_{CH} = 10^{-2}$, the strength of the effective electrostatic interactions among charged amino acids was still small but more comparable to the thermal energy (~10% of k_BT).

We conducted simulations for both Aβ_{1-40} and Aβ_{1-42} at effective electrostatic potential energies of $E_{CH} = 10^{-6}$ and 10^{-2} following the same protocol as for $E_{CH} = 0$. We then determined the oligomer size distributions and compared them to the case of $E_{CH} = 0$ (Figure 2). Surprisingly, the slight changes in interaction schemes among the three cases resulted in significant changes in the oligomer size distributions. Decreasing the amount of hydrophilic repulsion among the charged hydrophilic residues by increasing E_{CH} from 0 to 10^{-6} resulted in significantly increased numbers of larger oligomers for both Aβ_{1-40} and Aβ_{1-42}. Increasing the effective electrostatic interaction energy further (to 10^{-2}) resulted in another, though less pronounced, increase in the frequency of larger oligomers for both alloforms.

Why do effective electrostatic interactions have such a strong effect on oligomer size when they do not seem to affect monomer folding?[34] If one compares the DMD results with experimental data,[9] then the best agreement is obtained with $E_{CH} = 0$, a condition under which charged residues are treated as noncharged and hydrophilic. This result can be understood if, in the initial stages of oligomer formation, the charged side-chain groups were effectively screened by water molecules, resulting in the absence of effective electrostatic interactions among the charged amino acids. These results demonstrate that initial oligomer formation is driven primarily by a hydrophobic collapse and that electrostatic interactions may become important only after the desolvation of charged amino acid groups. Note that neither the Aβ_{1-40} nor the Aβ_{1-42} oligomer size distribution demonstrated the presence of oligomers of order $n > 15$. In contrast, the Aβ_{1-42} size distribution in the cases of $E_{CH} = 10^{-6}$ and 10^{-2} displayed a few peaks in the range of $n > 15$ (Figure 2b). Most of these peaks were associated with a standard error equal to the mean value of the occurrence probability, suggesting that these larger oligomers were a result of statistical fluctuations. It is significant, nonetheless, that such fluctuations were not present in the $E_{CH} = 0$ case. In the $E_{CH} = 10^{-2}$ case, the Aβ_{1-42} oligomer size distribution exhibited a peak at $n = 28$ with the standard error somewhat smaller than the mean occurrence probability value, marking the onset of Aβ_{1-42} assembly into larger oligomers (Figure 2b). An inspection of the Aβ_{1-42} conformations at $n = 28$ confirmed that electrostatic interactions between charged residues increased the rate of conversion of quasispherical Aβ_{1-42} oligomers (characteristic of $E_{CH} = 0$) to elongated protofibril-like (characteristic of $E_{CH} = 10^{-2}$) conformers (Figure 3).

Why was the formation of protofibril-like oligomers enhanced in the presence of electrostatic interactions? To answer this question, we first looked at the structural characteristics of monomeric and oligomeric assemblies regardless of particular assembly states and distributions of oligomer size. We analyzed the overall secondary structure to determine the structural changes resulting from different treatments of charged amino acids within the interaction schemes above. The major secondary structure component was the β-strand. We thus compared $\langle\beta$-strand$\rangle$ among all Aβ_{1-40} and Aβ_{1-42} trajectories at time frames

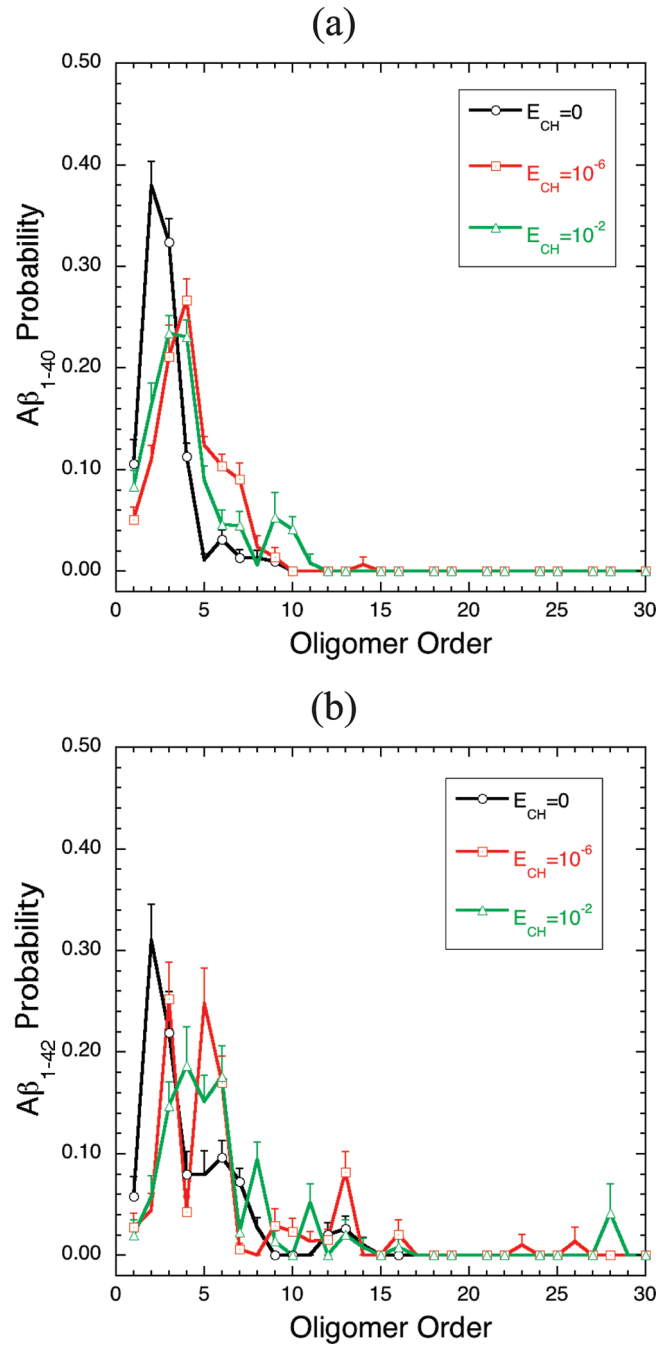

Figure 2. Oligomer size distributions for (a) Aβ_{1-40} and (b) Aβ_{1-42} obtained by DMD simulations using the four-bead protein model at $T = 0.130$ at different effective electrostatic interactions. Each distribution is an average over eight 20×10^6 simulation steps long trajectories. All conformations for time frames of 19×10^6, 19.5×10^6, and 20×10^6 simulation steps were included in the analysis. Each trajectory involved 32 peptides, initially spatially separated and each in a random coil conformation, enclosed in a 25-nm-length cubic box. The error bars represent SEM.

from 19×10^6 to 20×10^6 simulation steps for all three E_{CH} values (Table 2). Despite a trend toward a higher $\langle\beta$-strand$\rangle$ with higher E_{CH}, the differences were not significant. The observed formation of larger oligomers thus was not accompanied by a significant increase in $\langle\beta$-strand$\rangle$.

Dimer formation is the initial step in assembly. We thus explored the solvent-exposed surface area (SASA) of Aβ_{1-40} and Aβ_{1-42} dimers that were present in all trajectories at time frames between 19 and 20×10^{-6} simulation steps (Supporting

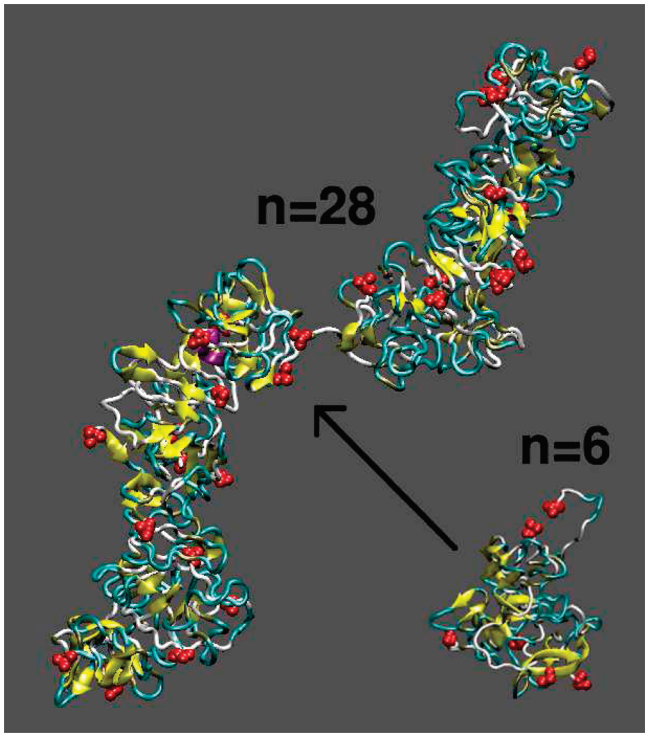

Figure 3. Effective electrostatic interactions speed up the conversion from hexamers ($n = 6$) to elongated protofibrillar assemblies (e.g., $n = 28$). β-Strands are depicted as yellow ribbons, turns as light-blue ribbons, and random coils as white ribbons. Amino acid D1, marking the N-termini, is represented by red spheres.

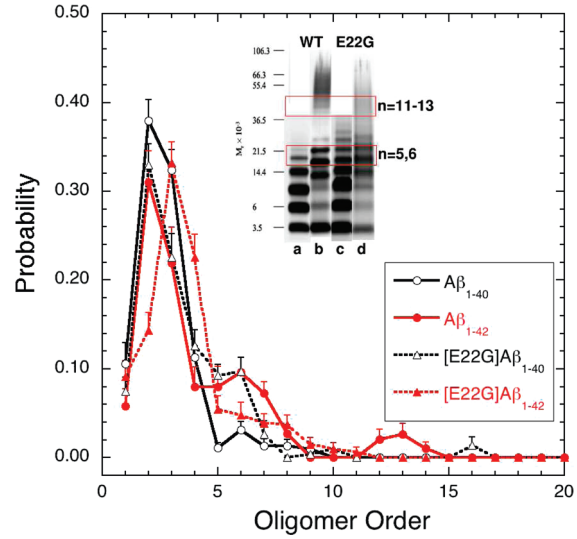

Figure 4. Oligomer size distributions for Arctic mutants [E22G] $A\beta_{1-40}$ (dotted black curve) and [E22G] $A\beta_{1-42}$ (dotted red curve) obtained by DMD simulations using the four-bead protein model at $T = 0.130$. Each distribution is an average over eight 20×10^6 simulation steps long trajectories. The oligomer size distributions for $A\beta_{1-40}$ (solid black curve) and $A\beta_{1-42}$ (solid red curve) are shown for comparison. All conformations for time frames of 19×10^6, 19.5×10^6, and 20×10^6 simulation steps were included in the analysis. Each trajectory involved 32 peptides, initially spatially separated and each in random coil conformation, enclosed in a 25-nm-length cubic box. The error bars represent SEM. The inset adapted from Bitan *et al.*[13] shows the experimental data obtained by PICUP/SDS-PAGE for (a) $A\beta_{1-40}$, (b) $A\beta_{1-42}$, (c) [E22G] $A\beta_{1-40}$, and (d) [E22G] $A\beta_{1-42}$.

Information, Figure S5). In all dimers, the amino acids or peptide segments most exposed to the solvent were D1, H6-S8, H13-Q15, E22, and S26-K28. Note that in all cases, with the exception of H13-Q15, one amino acid that is charged at neutral pH was present (D1, D7, E22, and K28). Among these, the only positively charged amino acid, K28, is in the turn region. The overall exposure to solvent was not drastically affected by the presence of electrostatic interactions. However, a more detailed comparison of the SASA for $A\beta_{1-40}$ and $A\beta_{1-42}$ dimers at $E_{CH} = 0$ showed that the $A\beta_{1-42}$ dimers had a significantly higher SASA in the A2-R5 region whereas H6 and E11 in $A\beta_{1-40}$ dimers were more exposed (Supporting Information, Figure S5a,b, black curves). We point out that the inclusion of electrostatic interactions did not change the SASA of the $A\beta_{1-40}$ dimers significantly (Supporting Information, Figure S5a) whereas it decreased the SASA of the $A\beta_{1-42}$ dimers in the N-terminal region (Supporting Information, Figure S5b). This suggests that the charged N-termini of $A\beta_{1-42}$ may participate in peptide assembly at $E_{CH} > 0$. These results also suggest that the formation of protofibril-like assemblies (Figure 3), which was enhanced by the presence of electrostatic interactions, may be driven by a desolvation process that enables salt bridge formation between the most exposed charged amino acids of the proximate oligomers.

Oligomer Size Distribution of Arctic Aβ. The similarity of the oligomer frequency distributions produced computationally (Figure 1) and experimentally[9] supports the use of our DMD approach to examine the effects of single amino acid Aβ substitutions causing familial forms of Alzheimer's disease (FAD). The Arctic E22G amino acid substitution produces $A\beta_{1-40}$ and $A\beta_{1-42}$ alloforms whose folding pathways resemble that of $A\beta_{1-42}$ but not that of $A\beta_{1-40}$. Here, we explore the effects of the Arctic substitution on oligomerization. We find that [E22G]$A\beta_{1-40}$ oligomerization involves an increased number of pentamers and hexamers (Figure 4, black dotted curve), comparable in number to those formed by $A\beta_{1-42}$ (Figure 4, red solid curve). No significant peaks at higher oligomer order were found. In [E22G]$A\beta_{1-42}$, the number of pentamers and hexamers was slightly decreased relative to the number for $A\beta_{1-42}$ and no peaks for decamers or higher-order oligomers were observed (Figure 4, red dotted curve). However, at longer simulation times ($(39-40) \times 10^6$) the relative number of [E22G]$A\beta_{1-42}$ hexamers became comparable to the relative number of $A\beta_{1-42}$ hexamers mainly because the relative number of $A\beta_{1-42}$ hexamers decreased as the relative number of $A\beta_{1-42}$ dodecamers increased (Supporting Information, Figure S1). Dimers were the most abundant conformers in $A\beta_{1-40}$, $A\beta_{1-42}$, and [E22G]$A\beta_{1-40}$, followed by trimers. Interestingly, [E22G]$A\beta_{1-42}$ was characterized by an increased number of trimers, followed by a slightly lower frequency of dimers. These size distribution characteristics agree well with the experimental findings.[13]

We also addressed the time evolution of all four size distributions and compared the individual statistical properties within and among distributions (Figures S1 and S2 and Table S1, Supporting Information). The results displayed in Figures S1 and S2 and Table S1 demonstrate that the oligomer size distributions, which were initially the same (one peak at oligomer size 1), developed into four statistically significantly different distributions, characteristic of the peptide under study, within the first 20×10^6 time steps. On the time scale between 20×10^6 and 40×10^6 time steps, all distributions retained their characteristics while demonstrating a slow evolution toward larger assemblies. The results of our analysis are consistent with a view that oligomers represent metastable, slowly evolving

states on the pathway to larger assemblies and not fixed states, frozen in time. Timescales that would allow for an observation of statistically significant numbers of assemblies of order $n > 20$ might be larger than 100×10^6 time steps and might require larger-scale simulations with an order-of-magnitude larger number of peptides per trajectory.

Structural Characterization of Wild-Type and Arctic Aβ Oligomers. We explored here the initial oligomerization of WT and Arctic (E22G) peptides of Aβ_{1-40} and Aβ_{1-42} using the interaction scheme $E_{CH} = 0$. This scheme yielded oligomer size distributions for Aβ_{1-40} and Aβ_{1-42} that agreed best with experimental results.[9] The scheme also revealed an initial hydrophobic collapse phase, during which low-order oligomers form but before the desolvation of the charged amino acids promotes further assembly into protofibrils.

The structure of monomers and oligomers could be described predominately as collapsed coils with β-strands separated by turns and loops as the dominant secondary structural element. This result is consistent with the NMR data derived by Zhang et al., showing that Aβ adopts a collapsed coil structure in water.[40] For each of the four peptides, we calculated the β-strand and turn propensities per residue for monomers alone and for each separate oligomer order, taking into account all conformations at time frames between 19×10^6 and 20×10^6 simulation steps (Figure 5). The average β-strand propensity across monomers and oligomers of order two (dimers) to six (hexamers) for all four peptides was 11−22% (Figure 5a). For Aβ_{1-40}, Aβ_{1-42}, and [E22G]Aβ_{1-40}, $\langle\beta$-strand$\rangle$ was lowest in the monomer state and increased the most upon monomer-to-dimer transition. This observation is qualitatively similar to the observation of Ono *et al.,* who studied cross-linked Aβ_{1-40} monomers, dimers, trimers, and tetramers and suggests that structural differences between monomers and dimers are larger than the differences among low-molecular-weight oligomers of order $n > 2$.[59] For each peptide individually, the relative increase in $\langle\beta$-strand$\rangle$ from the monomeric to hexameric oligomer state was significant as indicated by nonoverlapping SEM bars and amounted to 32, 39, 70, and 35% for Aβ_{1-40}, Aβ_{1-42}, [E22G]Aβ_{1-40}, and [E22G]Aβ_{1-42}, respectively. The increase was the most prominent in [E22G]Aβ_{1-40} even though the largest amount of $\langle\beta$-strand$\rangle$ in hexamers was observed for [E22G]Aβ_{1-42}, which also had significantly larger amounts of $\langle\beta$-strand$\rangle$ in a monomeric state compared to the other three peptides. The average turn propensity was 40−50% in all peptides (Figure 5b) and did not change significantly with oligomer order in Aβ_{1-40}, Aβ_{1-42}, or [E22G]Aβ_{1-40}. In [E22G]Aβ_{1-42}, however, we observed a significant (20%) decrease in the average turn propensity from the monomeric state (48.5 ± 3.5%) to the hexameric state (40.5 ± 2.9%).

Dimer formation is the first step in oligomer formation, but it has been suggested that pentamers and hexamers of Aβ_{1-42} play a key role in Aβ_{1-42} toxicity. We thus examined the β-strand propensity per amino acid in dimers (Figure 6a) and hexamers (Figure 6b) of all four peptides under study. The most striking difference between the β-strand propensities per residue among the four peptides was the presence of a short β-strand at A2-F4 in Aβ_{1-40} oligomers (Figure 6 a,b, black solid curves) that was completely absent in oligomers of the other three peptides (Figure 6, red solid and all dotted curves). This feature was shown previously to distinguish Aβ_{1-40} folded monomer structure from the folded monomer structures of Aβ_{1-42}, [E22G]Aβ_{1-40}, and [E22G]Aβ_{1-42}.[34] The present data demonstrated that in Aβ_{1-40}, β-strand propensities at A2-F4 increased upon oligomerization and were highest in hexamers, suggesting that this region plays a significant role in Aβ_{1-40} oligomer assembly. We carried out a detailed pairwise comparison of the $\langle\beta$-strand$\rangle$ per residue and described it in the Supporting Information (Figure S4). To examine further the significance of the A2-F4 β-strand in Aβ_{1-40} oligomer formation, we studied the time evolution of the interaction between a tetramer and dimer during Aβ_{1-40} hexamer formation (Figure 8). A short parallel intermolecular β-strand (A2-F4) in a dimer (upper right)

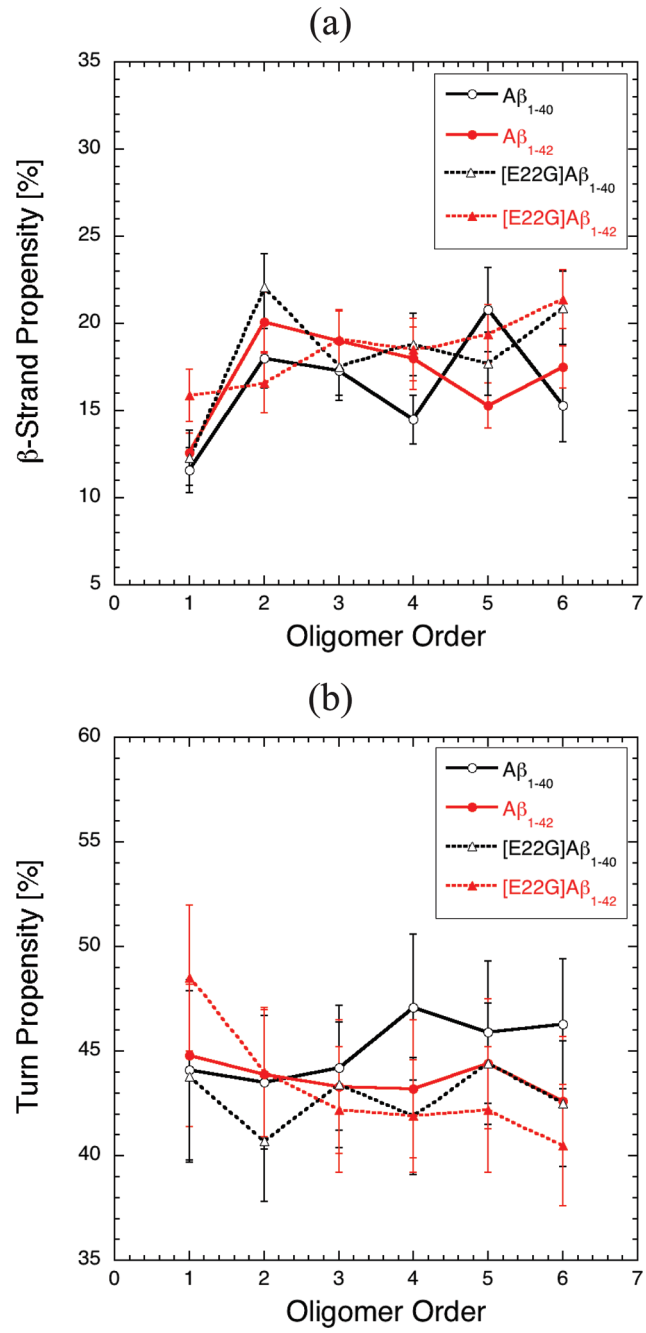

Figure 5. Average propensities for (a) a β-strand and (b) turn formation in monomers, dimers, trimers, tetramers, pentamers, and hexamers for Aβ_{1-40} (solid black curve), Aβ_{1-42} (solid red curve), [E22G]Aβ_{1-40} (dotted black curve), and [E22G]Aβ_{1-42} (dotted red curve). The error bars correspond to SEM.

(59) Ono, K.; Condron, M. M.; Teplow, D. B. *Proc. Natl. Acad. Sci. U.S.A.* **2009**, *106*, 14745–14750.

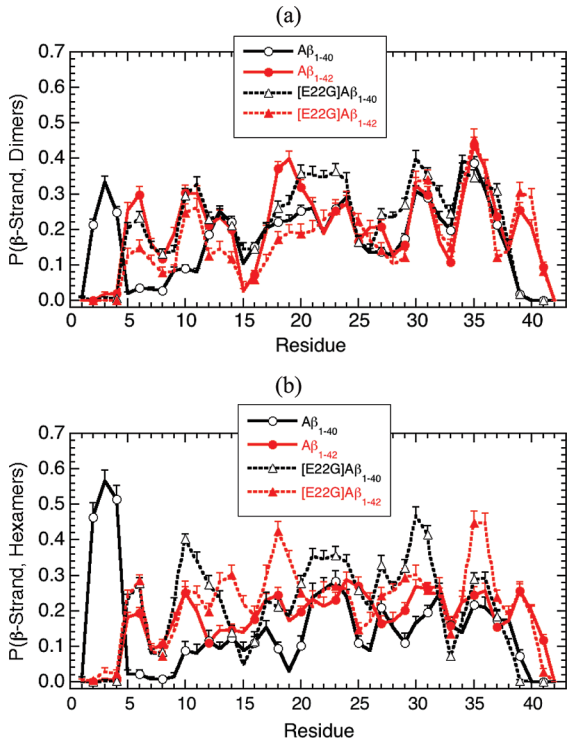

Figure 6. Average β-strand propensity per amino acid for (a) dimers and (b) hexamers of $A\beta_{1-40}$ (solid black curve), $A\beta_{1-42}$ (solid red curve), [E22G]$A\beta_{1-40}$ (dotted black curve), and [E22G]$A\beta_{1-42}$ (dotted red curve). The error bars correspond to SEM.

interacts with one of the N-terminal regions in the tetramer (lower left). Initially, the N-terminal region docked onto the existing β-sheet (Figure 8A) and eventually adopted a β-strand structure (Figure 8B). This process was particular to $A\beta_{1-40}$ hexamer formation and was observed in 13 out of 24 $A\beta_{1-40}$ hexamers across different trajectories and time frames. Oligomerization of the other three peptides was not accompanied by the formation of β-strands, and the merging of two conformers into a larger one happened on timescales smaller than 0.1×10^6 (time between the saved simulation frames).

To gain insight into the effect of the Arctic mutation on the solvent exposure of different regions of the peptides, we calculated the average SASA per residue in dimers (Supporting Information, Figure S5a) and hexamers (Supporting Information, Figure S5b) for all four peptides. The results indicated that the overall structures of the C-terminal halves of the peptides comprising the oligomers were the same in all four peptides. Regions CHC, MHR, and CTR comprised the oligomer core, which was the most shielded from the solvent. In hexamers, the oligomer core had, on average, smaller SASAs than in dimers, suggesting that the hexamer core was more shielded from the solvent than the dimer core. SASAs in the N-terminal region were not affected by the higher oligomer order but differed among the four peptides. Differences in SASA among the four peptides were observed in N-terminal region D1-R5, where $A\beta_{1-40}$ oligomers showed significantly lower SASAs relative to oligomers of the other three peptides. This result was consistent with the existence of the β-strand structure at A2-F4 in only $A\beta_{1-40}$ oligomer structures, resulting in lower SASAs caused by the involvement of the A2-F4 region in intra- and intermolecular contacts. An important observation was that SASAs of N-terminal region D1-R5 within $A\beta_{1-42}$, [E22G]$A\beta_{1-40}$, and [E22G]$A\beta_{1-42}$ were similar to each other and were all significantly higher than the corresponding SASAs in $A\beta_{1-40}$. Unlike $A\beta_{1-40}$, the other three peptides possessed N-termini that did not appear to be involved in intra- and intermolecular contacts and were thus mostly unstructured.

To gain additional insight into amino acid geometry within oligomers, we calculated the average relative distance from the center of mass per residue (Figure 9). First, we estimated the dimer and hexamer average sizes by identifying the largest relative distance from the center of mass. Twice the value of this distance was used to estimate the average diameter of dimers (Figure 9a), $d_2 \approx 3$ nm, and the average dimer of hexamers (Figure 9b), $d_6 \approx 4.6$ nm. The average hexamer diameter was slightly larger than ~4.3 nm calculated by using the dimer diameter (3 nm), assuming that the number of peptides n in an oligomer scaled with its volume $V \propto d^3$ as $n \propto d^3$, where d was the diameter of the oligomer of order n. This could be explained by taking into account the shape variability of hexamers, which was in many cases more elongated than spherical (in contrast to more consistently spherical dimers), resulting in increased relative distances from the center of mass. This particular scaling of the oligomer size from dimers to hexamers, resulting in less densely packed hexamers relative to dimers, is in agreement with the observed nonlinear increase in oligomer sizes with oligomer order n in cross-linked $A\beta_{1-40}$ monomers, dimers, trimers, and tetramers in a recent study by Ono et al.[59] Our observation of oligomer shapes ranging from spherical to elongated ellipsoidal is also consistent with earlier neutron-scattering data demonstrating a prolate ellipsoid shape for Aβ oligomers.[60]

Second, we compared the relative arrangement of different peptide regions with respect to the center of mass within dimers and hexamers. Except in N-terminal region A1-Y10, the relative arrangement of residues was similar for all four peptides in dimers (Figure 9a). Region A1-R5 of $A\beta_{1-40}$ dimers was characterized by significantly lower relative distances than those of $A\beta_{1-42}$, [E22G]$A\beta_{1-40}$, and [E22G]$A\beta_{1-42}$ dimers (Figure 9a). In dimers of the two shorter peptides, $A\beta_{1-40}$ and [E22G]$A\beta_{1-40}$, region V18-F20 was the closest to the center of mass (at ~0.5 nm). In dimers of the two longer peptides, $A\beta_{1-42}$ and [E22G]$A\beta_{1-42}$, I41 was the closest to the center of mass (at ~0.4 nm). Peptide region D7-G9 was characterized by the longest distance of ~1.5 nm from the center of mass in dimers of all four peptides.

Relative distances at A1-R5 were significantly larger in $A\beta_{1-42}$ hexamers than in $A\beta_{1-40}$ hexamers, and distances at A1-R5 of both Arctic hexamers fell between those of $A\beta_{1-40}$ and $A\beta_{1-42}$ hexamers (Figure 9b). Region D7-S8 had the largest relative distance from the center of mass in hexamers of all four peptides (~2.3 nm). D1 of $A\beta_{1-42}$ hexamers was also at the same distance of ~2.3 nm. These differences in the relative distances between the four peptides were consistent with the SASA results, which demonstrated significant differences in solvent exposure in the N-terminal region of dimers and hexamers (Supporting Information, Figure S5a,b).

$A\beta_{1-40}$ hexamers were characterized by the minimal distance of ~1.4 nm at V40 and slightly larger distances of ~1.5 nm at V18-F20, which were, unlike in dimers, significantly higher than in hexamers of the other three peptides (Figure 9b, black solid curve). The cause of relatively large distances at V18-F20 from

(60) Yong, W.; Lomakin, A.; Kirkitadze, M. D.; Teplow, D. B.; Chen, S. H.; Benedek, G. B. *Proc. Natl. Acad. Sci. U.S.A.* **2002**, *99*, 150–154.

the center of mass in Aβ_{1-40} hexamers was the existence of a substantial number of Aβ_{1-40} hexamer conformations similar to the one shown in Figure 8, where a hexamer consisted of two distinct interacting spherical oligomers of lower order (in Figure 8, a dimer and a tetramer). In Aβ_{1-42} hexamers, V40-I41 and L34-M35 were closest to the center of mass with relative distances of ~1.2 nm (Figure 9b, red solid curve). The relative distances at I31-A42 of [E22G]Aβ_{1-40} and [E22G]Aβ_{1-42} hexamers fell between the Aβ_{1-42} and Aβ_{1-40} curves (Figure 9b, black and red dotted curves). Here the relative distances of [E22G]Aβ_{1-40} hexamers were smaller than in [E22G]Aβ_{1-42} hexamers and thus more similar to distances found in Aβ_{1-42} hexamers (Figure 9b, red solid and black dotted curves). Relative distances in the I31-V40 (I31-A42) region were correlated with the compactness of the hexamers of the four peptides. The most compact were the Aβ_{1-42} hexamers, and the least compact were the Aβ_{1-40} hexamers for the reasons discussed above. Interestingly, between the two Arctic peptides, [E22G]Aβ_{1-42} hexamers were less compact, consistent with our observation that some conformations showed [E22G]Aβ_{1-42} hexamers composed of two interacting oligomers of lower order similar to Aβ_{1-40} hexamers. Unlike Aβ_{1-40} hexamers, however, the interaction between these two [E22G]Aβ_{1-42} oligomers did not proceed through the formation of β-strands at A2-F4.

Peptide Regions Involved in Aβ Oligomerization. To identify peptide regions that play key roles in oligomer formation, we quantified the tertiary and quaternary structures comprising Aβ oligomers. A comparison of regions identified within oligomer populations formed by each of the four peptides provided the means to elucidate the distinct structures and peptide regions mediating common and distinct assembly paths of the peptides. We computed the contact maps of dimers and hexamers for all four peptides (Supporting Information, Figures S6 and S7) and derived two types of contact maps. (See the Methods section.) Considering all contacts between each pair of amino acids, irrespective of the interaction type, we obtained intramolecular (Supporting Information, Figure S6, lower left triangles of all maps) and intermolecular (Supporting Information, Figure S7, lower left triangles of all maps) contact maps. In addition, we analyzed the backbone hydrogen bonding to be able to identify particular patterns of secondary structure formation within each molecule (intramolecular) or among molecules (intermolecular). These intramolecular (Supporting Information, Figure S6, upper right triangles of all maps) and intermolecular (Supporting Information, Figure S7, upper right triangles of all maps) maps contain hydrogen bond propensities for each pair of residues.

A detailed description of contact maps is given in Tertiary and Quaternary Structures of Aβ Oligomers in Supporting Information. The comparisons made in Supporting Information provide a large amount of structural information. Aβ_{1-40} and Aβ_{1-42} oligomers were the most distinct structurally. [E22G]Aβ_{1-40} and [E22G]Aβ_{1-42} oligomers shared characteristics with oligomers formed by both WT peptides. Our analyses revealed a number of important structural characteristics of the oligomers:

1. The tertiary structures of peptides comprising oligomers of all four peptides were characterized by a hydrogen bonding pattern consistent with a small, but nonzero, α-helix propensity in the G25-G33 region. The propensity was higher and involved a more lengthy peptide segment (G22-G33) in both Arctic peptides.
2. Aβ_{1-40} oligomer formation proceeded predominantly through interactions among the CHC regions and intermolecular β-strand formation in the A2-F4 N-terminal region.
3. Aβ_{1-42} oligomer formation proceeded predominantly through intermolecular interactions involving the I31-A42 C-terminal regions as well as interactions between I31-A42 and the CHC region.
4. Aβ_{1-40} dimers and hexamers had indistinguishable tertiary structures. In contrast, the average number of intramolecular (tertiary structure) contacts in Aβ_{1-42} hexamers was smaller than in Aβ_{1-42} dimers.
5. [E22G]Aβ_{1-40} oligomer formation proceeded predominantly through intermolecular interactions between the I31−V40 C-terminal region and the CHC. Intermolecular contacts among the CHC regions as well as contacts among the I31-V40 regions were stronger than in Aβ_{1-40} and weaker than in Aβ_{1-42}.
6. [E22G]Aβ_{1-42} oligomerization involved intermolecular contacts in the I31-V40 C-terminal region as well as contacts between the CHC and I31-V40. In addition, the A2-F4 region participated in intermolecular contacts with the CHC and I31-A42 more than in Aβ_{1-42} and [E22G]Aβ_{1-40} but less than in Aβ_{1-40}.
7. As with Aβ_{1-42} but not with Aβ_{1-40}, a loss of tertiary structure contacts was observed during the assembly transition of [E22G]Aβ_{1-40} from dimer to hexamer, but the effect was smaller than that observed with Aβ_{1-42}.
8. In contrast to the other three peptides, a small increase in the number of tertiary structure contacts was observed during the transition of [E22G]Aβ_{1-42} from dimer to hexamer.

These observations demonstrate that the balance of intra- and, in particular, intermolecular interactions among different peptide regions determines the oligomerization propensity of the four peptides. Aβ_{1-42}, in which the center of intermolecular interactions was the C-terminal region, formed larger oligomers compared to Aβ_{1-40}, where the center of intermolecular interactions was the CHC region (with additional strong participation of the A2-F4 region). The strongest intermolecular interactions in [E22G]Aβ_{1-40} hexamers also involved the C-terminal I31-V40 region but to a lesser extent than in Aβ_{1-42}. Correspondingly, the oligomerization propensity was less than in Aβ_{1-42} but more than in Aβ_{1-40}. The observed oligomerization tendencies of [E22G]Aβ_{1-42} were consistent with the above results. Here, the intermolecular interactions were centered more at the CHC than at I31-A42, and thus its oligomerization propensity was between that of [E22G]Aβ_{1-40} and that of Aβ_{1-40}.

Formation of Higher-Order Aβ_{1-42} Oligomers. It has been suggested recently that Aβ dodecamers are the proximate neurotoxins in AD.[12,61] We examined the structure of dodecamers of Aβ_{1-42}, the only peptide in our study that displayed significant numbers of oligomers of order 11−13 at $E_{CH} = 0$, the implicit solvent parameter that best described Aβ oligomerization. We showed that even small effective electrostatic interactions ($E_{CH} = 10^{-2}$) induced the formation of elongated protofibril-like assemblies. We thus asked whether Aβ_{1-42} dodecamers obtained at $E_{CH} = 0$ or undecamers obtained at $E_{CH} = 10^{-2}$ [62] were structurally similar or distinct. Assuming that

(61) Lesné, S.; Koh, M. T.; Kotilinek, L.; Kayed, R.; Glabe, C. G.; Yang, A.; Gallagher, M.; Ashe, K. H. *Nature* **2006**, *440*, 352–357.
(62) Under these conditions, an insufficient number of dodecamers were observed to allow further analysis.

undecamers at $E_{CH} = 10^{-2}$ were representative of the protofibrillar structure and dodecamers at $E_{CH} = 0$ were representative of oligomeric structure, this comparison would help elucidate structural changes involved in the assembly from oligomers to protofibrils.

Tertiary structures of Aβ_{1-42} dodecamers obtained at $E_{CH} = 0$ (Figure 10a) and Aβ_{1-42} undecamers obtained at $E_{CH} = 10^{-2}$ (Figure 10c) were similar in that the strongest intramolecular contacts involved the I31-A42 region. However, the contact strengths differed in all four regions as indicated by boxes (1−4). Dodecamers were characterized by significantly fewer tertiary structure contacts than protofibril-like undecamers (i) in the central folding region (Figure 10a,c, box 4) and (ii) in the A2-F4 N-terminal region interacting with the CHC, MHR, and CTR (Figure 10a,c, box 2).

Compared to Aβ_{1-42} hexamers, Aβ_{1-42} dodecamers had even fewer intramolecular contacts in the central folding region (Figure 10a, box 4), suggesting that additional unfolding of individual Aβ_{1-42} peptides was needed for their assembly into dodecamers. In contrast, tertiary contacts in the central folding region of protofibril-like undecamers resembled those of Aβ_{1-40} dimers and hexamers (Figure 10c, box 4) but were characterized by a larger number of hydrogen bonds (Figure 10c, box 4, upper right triangle). Tertiary contacts involving A2-F4 (Figure 10a, box 2) in Aβ_{1-42} dodecamers were stronger than the ones in Aβ_{1-42} hexamers but weaker than in protofibril-like undecamers (Figure 10c, box 2).

Quaternary structures of Aβ_{1-42} dodecamers obtained at $E_{CH} = 0$ (Figure 10b) and Aβ_{1-42} undecamers obtained at $E_{CH} = 10^{-2}$ (Figure 10d) also were different. The intermolecular contacts in regions enclosed in boxes 3−5 involving the CTR, MHR, and CHC were the strongest intermolecular contacts in both dodecamers and in protofibril-like undecamers. However, these contacts were generally stronger in the dodecamers than in the undecamers. The undecamers were characterized by additional intermolecular interactions involving the A2-F4 region (Figure 10d, boxes 1 and 2) that were also characteristic of Aβ_{1-40} hexamer formation (i.e., the existence of an intermolecular parallel β-strand (Figure 10 d, box 1)).

We also examined all four contact maps for the occurrence of any regular arrangement of hydrogen bonds (Figure 10 a−d, upper right triangle). An off-diagonal intramolecular hydrogen bond pattern consistent with nonzero α-helix propensities was found in both *intra*molecular contact maps of dodecamers (Figure 10a, upper right triangle) and protofibril-like undecamers (Figure 10c, upper right triangle) and was most prevalent in the G25-G33 regions. In addition, this pattern also was present in regions with high turn propensities (Figure 7), suggesting that the turn and α-helix propensities were correlated and were enhanced by the presence of glycines in the sequence. In addition, a diagonal *inter*molecular hydrogen bond pattern consistent with parallel in-register intermolecular hydrogen bonds was observed in undecamers at $E_{CH} = 10^{-2}$ (Figure 10d, upper right triangle). Even though the corresponding hydrogen bond propensities in this pattern were low, this feature might indicate the onset of a parallel cross-β structure that is characteristic for full-length Aβ and several other amyloid fibrils. The fact that this parallel intermolecular hydrogen bond pattern was most pronounced in protofibril-like undecamers[63] suggested that electrostatic interactions that become effective upon desolvation significantly contribute to the formation of the parallel in-register cross-β structure.

(63) [E22G]Aβ_{1-42} hexamers showed a similar though less pronounced pattern; see Supporting Information, Figure S5h, upper right triangle.

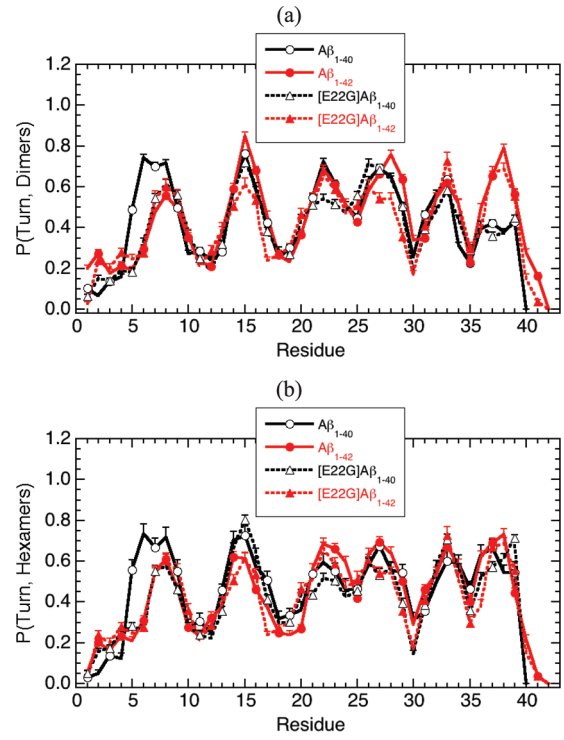

Figure 7. Average turn propensity per amino acid for (a) dimers and (b) hexamers of Aβ_{1-40} (solid black curve), Aβ_{1-42} (solid red curve), [E22G]Aβ_{1-40} (dotted black curve), and [E22G]Aβ_{1-42} (dotted red curve). The error bars correspond to SEM.

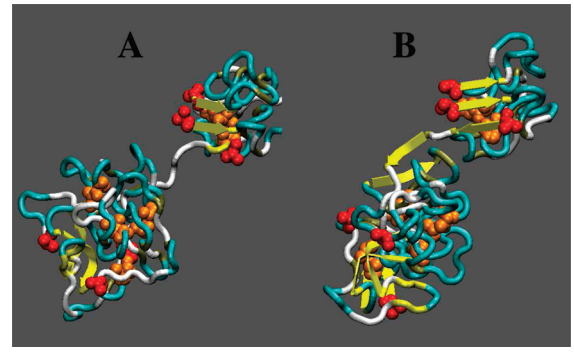

Figure 8. Formation of an Aβ_{1-40} hexamer from a tetramer and a dimer for (A) 19.0 × 10^6 and (B) 19.6 × 10^6 simulation steps. β-Strands are depicted as yellow ribbons, turns as light blue ribbons, and random coils as white ribbons. Amino acid D1, marking the N-termini, is represented by red spheres, and V39 and V40 are represented by orange spheres.

Discussion

Amyloid β-protein belongs to a class of amyloid-forming proteins whose assembly is thought to cause a variety of neurodegenerative diseases. It is hypothesized that less-structured oligomeric assemblies, that may be on- or off-pathway for amyloid fibril formation, are the most toxic structures triggering the disease.[64] Examples include but are not limited to α-synuclein, relevant to Parkinson's disease,[65] and islet

(64) Walsh, D. M.; Selkoe, D. J. *Protein Pept. Lett.* **2004**, *11*, 213–228.
(65) Irvine, G.; El-Agnaf, O. ; Shankar, G. ; Walsh, D. *Mol. Med.* **2008**, *14*, 451−464.

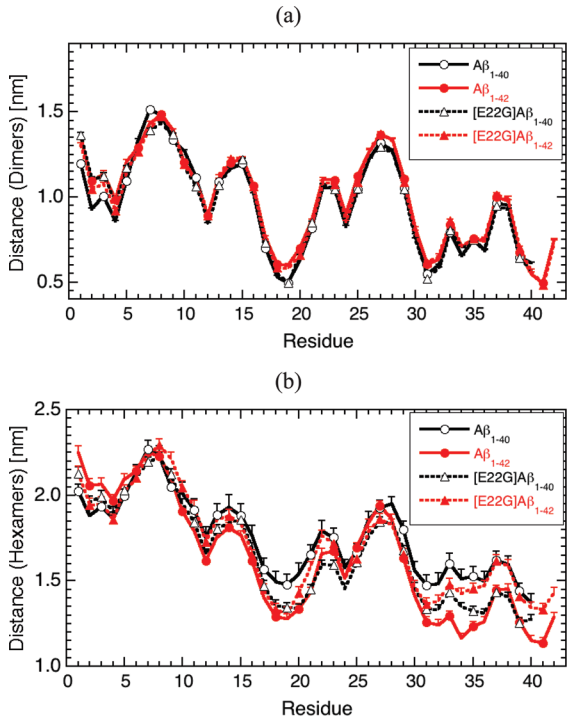

Figure 9. Relative distances of individual residues from the center of mass of Aβ_{1-40} (solid black curve), Aβ_{1-42} (solid red curve), [E22G]Aβ_{1-40} (dotted black curve), and [E22G]Aβ_{1-42} (dotted red curve) (a) dimers and (b) hexamers. The error bars correspond to SEM.

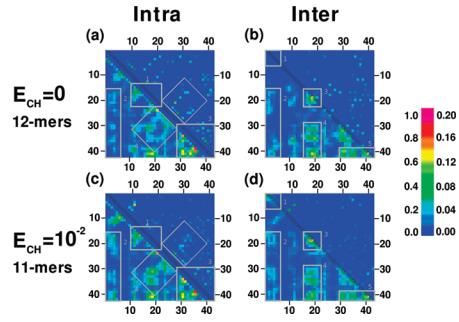

Figure 10. Intra- and intermolecular contact maps of Aβ_{1-42} oligomers: (a, b) $n = 12$ for $E_{CH} = 0$ (average taken over 12 conformers) and (c, d) $n = 11$ for $E_{CH} = 10^{-2}$ (average taken over 30 conformers). The lower triangle contains the average number of contacts between two amino acids, and the upper triangle contains the average number of hydrogen bonds for each pair of amino acids. The scale on the right shows the color mapping. The two types of maps have different scales: the scale on the left corresponds to the average number of contacts, and the scale on the right corresponds to the average number of hydrogen bonds. The two thin diagonal lines are drawn through the diagonal elements of the two types of contact maps. The rectangular gray boxes with numbers mark regions of interest.

amyloid polypeptide, relevant to type 2 diabetes.[66,67] Because toxicity is by definition directly associated with the structural properties of these protein assemblies, it is imperative to address the question of how such a mutation alters the structural properties of the protein under study and the pathway of protein assembly.

In the present work, we studied the oligomer formation of Aβ_{1-40}, Aβ_{1-42}, and their Arctic mutants [E22G]Aβ_{1-40} and [E22G]Aβ_{1-42} using the DMD approach combined with a four-bead protein model and implicit solvent. We examined oligomerization pathways of the four peptides, derived oligomer size distributions, and compared the distributions to in vitro data obtained by PICUP/SDS-PAGE.[10] *In vitro* oligomer size distributions of a series of Aβ peptides obtained by PICUP/SDS-PAGE were shown to be sensitive to the peptide length and sequence.[9,13,68] The oligomer size distribution thus can be considered to be a fingerprint of the peptide under study and a means to distinguish oligomerization pathways of different Aβ variants. We used these data to adjust the values of the two implicit solvent parameters (strengths of the effective hydropathic and electrostatic interactions) that would produce simulated oligomer distributions best matching those obtained experimentally. By incorporating a better estimate of physiological temperature and using longer simulation times relative to those in our earlier study,[31] we observed an Aβ_{1-42} oligomer size distribution that included not only a peak at pentamers/hexamers but also a peak at oligomer orders of 12 and 13, which was not observed in our prior work.[31]

The Arctic mutation causes a severe, early-onset form of AD.[39] The propensity of [E22G]Aβ_{1-40} and [E22G]Aβ_{1-42} to form paranuclei or higher-order oligomers may be a critical factor contributing to the pathogenesis of this form of AD. [E22G]Aβ_{1-42} toxicity also was demonstrated in a recent study by Luheshi *et al.,* who used the rational mutagenesis of Aβ_{1-42} to find a strong correlation between the aggregation propensity of a series of Aβ_{1-42} mutants and the dysfunction that they caused in a Drosophila model of Alzheimer's disease.[69] Among several Aβ_{1-42} variants, Arctic mutant [E22G]Aβ_{1-42} was characterized by strongly enhanced toxicity relative to that of Aβ_{1-42}, presumably caused by oligomeric forms of [E22G]Aβ_{1-42}.[69] To study the oligomerization of the two Arctic peptides, we applied our DMD simulation protocol to obtain a large population of *in silico* [E22G]Aβ_{1-40} and [E22G]Aβ_{1-42} oligomers. None of the Arctic mutants produced significant numbers of oligomers larger than nonamers, but [E22G]Aβ_{1-40} displayed a high probability of forming both pentamers and hexamers and [E22G]Aβ_{1-42} produced increased numbers of trimers and also small amounts of pentamers and hexamers. These results were consistent with PICUP/SDS-PAGE data, except for the frequency of [E22G]Aβ_{1-42} paranuclei, which was experimentally found to be similar to the frequency of Aβ_{1-42} paranuclei.[13] This apparent discrepancy was resolved by further extending the simulation time, during which the number of Aβ_{1-42} hexamers slightly decreased and the number of Aβ_{1-42} dodecamers increased, resulting in comparable relative numbers of Aβ_{1-42} and [E22G]Aβ_{1-42} paranuclei.

We also examined whether the probability distributions of oligomer sizes for each of the four peptides reached a steady state.[70] We quantified the changes in all four distributions due to time evolution on different timescales. Our data showed that by considering timescales of up to 5×10^6 simulation steps all four size distributions reached a metastable steady state within

(66) Nanga, R. P. R.; Brender, J. N.; Xu, J.; Veglia, G.; Ramamoorthy, A. *Biochemistry* **2008**, *47*, 12689–12697.
(67) Nanga, R. P. R.; Brender, J. N.; Xu, J.; Hartman, K.; Vivekanandan, S.; Ramamoorthy, A. *J. Am. Chem. Soc.* **2009**, *131*, 8252–8261.
(68) Bitan, G.; Tarus, B.; Vollers, S. S.; Lashuel, H. A.; Condron, M. M.; Straub, J. E.; Teplow, D. B. *J. Am. Chem. Soc.* **2003**, *125*, 15359–15365.
(69) Luheshi, L. M.; Tartaglia, G. G.; Brorsson, A. C.; Pawar, A. P.; Watson, I. E.; Chiti, F.; Vendruscolo, M.; Lomas, D. A.; Dobson, C. M.; Crowther, C. D. *PLoS Biol.* **2007**, *5*, e290.
(70) Although a true steady state of Aβ monomers and oligomers of different order may not exist, oligomer size distributions were experimentally observed to be stable in the time period prior to protofibril formation.

the first 15×10^6 time steps. However, slower time evolution on timescales of 20×10^6 was still observed, consistent with a view that oligomeric states represent quasi-stable intermediates, possibly on the pathway to protofibril and fibril formation.

We explored the role of electrostatic interaction in Aβ oligomerization and demonstrated that the oligomer size distribution was sensitive to electrostatic interactions among the charged amino acids. The best fit to experimental oligomer size distributions was obtained if the side-chain charges were completely neglected and the charged side chains were modeled as pure hydrophiles. These findings are consistent with the hypothesis that the formation of oligomers is driven by a hydrophobic collapse, during which water interacting with the hydrophilic side chains efficiently solvates the charged residues, inhibiting the electrostatic interactions among them. We further showed that if the charged side chains were allowed to interact electrostatically then the spherical oligomers readily evolved into elongated protofibrils, even at very small strength of the effective electrostatic interaction. We showed that this mechanism was a consequence of the structural properties of quasispherical oligomers, which were characterized by strong exposure to the solvent of charged residues at the N-terminus (D1, E3, R5, and D7) and in the A21-A30 turn region (E22, D23, and K28).

We then structurally analyzed spherical oligomers produced by the four different peptides. As shown previously, $A\beta_{1-40}$ and $A\beta_{1-42}$ oligomers were characterized by significant differences in β-strand and turn propensities in the D1-Q15 N-terminal region, even though their sequences differ at the C-termini.[31] We showed that the secondary structure propensities at the N-termini of oligomers of both Arctic mutants resembled the propensities of $A\beta_{1-42}$ but not those of $A\beta_{1-40}$. Thus, an amino acid substitution at the CHC (E22G) gives rise to structural differences in another region, the N-terminus. These results are consistent with a view that Aβ conformations are significantly affected by the competition between the N- and C-termini to form a stable complex with the CHC.[71] $A\beta_{1-42}$ oligomer formation was predominantly driven by intermolecular interactions among the CTRs whereas in $A\beta_{1-40}$ assembly the intermolecular interactions among the CHC regions were dominant. For the Arctic peptides, intermolecular interactions among the CTRs and CHC regions were equally important. Of the four peptides, only $A\beta_{1-40}$ oligomerization was characterized by the involvement of the A2-F4 N-terminal region in intermolecular interactions. We showed that $A\beta_{1-40}$ hexamers assembled from oligomers of lower order through the formation of a parallel β-strand at A2-F4, which appeared to be the rate-limiting process. This observation is consistent with existing PICUP/SDS-PAGE data demonstrating that N-terminally truncated $A\beta_{3-40}$ and $A\beta_{5-40}$ (in which parallel β-strand formation at A2-F4 would be hindered or nonexistent) displayed increased numbers of pentamers/hexamers whereas $A\beta_{3-42}$ and $A\beta_{5-42}$ oligomer size distributions were indistinguishable from that of $A\beta_{1-42}$.[13] Further examination of the intra- and intermolecular contacts between different peptide regions in each peptide demonstrated that [E22G]$A\beta_{1-40}$ hexamers were structurally similar to $A\beta_{1-42}$ hexamers, implicating the [E22G]$A\beta_{1-40}$ hexamers in this familial form of AD. Considering that the shorter Aβ alloform is typically more abundant in the human body, the ability of [E22G]$A\beta_{1-40}$ to form toxic oligomers might play a critical role in this familial form of AD.

We systematically examined the intra- and intermolecular hydrogen bonds in oligomers of all four peptides. The tertiary structure of all four peptides was characterized by a hydrogen bonding pattern consistent with low α-helix propensities in the G25-G33 region that were more pronounced in the G22-G33 region of both Arctic peptides. Glycines were also associated with increased turn propensities, so our data showed a correlation between the turn and α-helix propensities in all four peptides. This observation is consistent with *in vitro* findings that Aβ assembly into protofibrils and fibrils is preceded by a transitory increase in the α-helix structure.[43] We also examined $A\beta_{1-42}$ dodecamers, which recently were suggested to be the proximate neurotoxic species in AD.[12,61] Similar α-helix propensities were observed in $A\beta_{1-42}$ dodecamers and in elongated protofibrillar $A\beta_{1-42}$ undecamers obtained at protofibril-inducing nonzero electrostatic interaction potentials. Interestingly, in elongated protofibrillar $A\beta_{1-42}$ undecamers, we observed a parallel intermolecular hydrogen bond pattern that was consistent with the onset of parallel, in-register cross-β structure characteristic of full-length Aβ fibrils.

Our computational findings are consistent with the existence of three distinct processes occurring sequentially within a single Aβ assembly pathway: (1) fast hydrophobic collapse resulting in a population of oligomers; (2) slow desolvation enabling charged residues to interact electrostatically and thus induce the formation of elongated protofibrils; and (3) very slow emergence of parallel in-register intermolecular hydrogen bonding associated with the cross-β structure of the amyloid fibril. Whether such an on-pathway scenario exists *in vitro* or *in vivo* and whether this scenario represents the only possible pathway of assembly may be critical to understanding all amyloid-forming proteins. Experimental testing of the assembly pathway might be possible by further developing spectroscopic techniques that would allow the observation of Aβ oligomerization in an unperturbed solvent on subsecond timescales in a time-resolved manner and with spatial resolution of at least a nanometer, such as time-resolved liquid transmission electron microscopy.[72]

The two processes that we discussed within the scope of the present study (i.e., hydrophobic collapse and slow desolvation) originate in an explicit aqueous environment in the way water molecules interact with hydrophobic versus hydrophilic residues. Effective hydropathic and electrostatic interactions are caused or strongly affected by the polar nature of water molecules and their ability to form hydrogen bonds among themselves and with hydrophilic protein groups.[73] Thus, both processes are directly related to the thermodynamics and dynamics of water. Here, hydrophobic collapse refers to a process during which the hydrophobic groups minimize their exposure to water in order to maximize the number of hydrogen bonds among water molecules, which is energetically favorable. Because water molecules do not form hydrogen bonds with hydrophobic protein groups, this process is expected to occur rapidly. However, the desolvation of hydrophilic residues requires water molecules to break hydrogen bonds with hydrophilic residues, which is energetically unfavorable, resulting in longer times needed for desolvation.

(71) Maji, S.; Loo, R. O.; Inayathullah, M.; Spring, S.; Vollers, S.; Condron, M.; Bitan, G.; Loo, J.; Teplow, D. *J. Biol. Chem.* **2009**, *284*, 23580–23591.

(72) de Jonge, N.; Peckys, D. B.; Kremers, G. J.; Piston, D. W. *Proc. Natl. Acad. Sci. U.S.A.* **2009**, *106*, 2159–2164.

(73) Finkelstein, A. V.; Ptitsyn, O. B. *Protein Physics: A Course of Lectures*; Academic Press: London, 2002.

Our present results demonstrate that the timescale over which hydrophobic collapse occurs is sensitive to the Aβ length and to single amino acid substitutions. The process of desolvation with respect to Aβ_{10-35} monomer conformation was studied using all-atom MD by Massi and Straub,[74] who showed that the amino acid substitution associated with the Dutch mutation (E22Q) induced changes in the first solvation layer of water that resulted in enhanced desolvation, a key process in assembly. Recently, all-atom MD simulations of two amyloidogenic protein fragments were carried out to monitor desolvation occurring upon addition of a monomer to a preformed fibril.[75] Consistent with our data, Reddy *et al.* suggest that the desolvation process, which is protein-sequence-dependent, plays an important role in fibril formation.[75] We demonstrated that our DMD approach captures the majority of distinct characteristics of Aβ_{1-40}, Aβ_{1-42}, [E22G]Aβ_{1-40}, and [E22G]Aβ_{1-42} oligomer size distributions, provides mechanistic insights into elongated protofibril formation, and provides structural information on toxic Aβ oligomers relevant to structure-based drug design.

(74) Massi, F.; Straub, J. E. *Biophys. J.* **2001**, *81*, 697–709.
(75) Reddy, G.; Straub, J. E.; Thirumalai, D. *Proc. Natl. Acad. Sci. U.S.A.* **2009**, *106*, 11948–11953.

Acknowledgment. This research was supported by NIH grant AG027818.

Supporting Information Available: Time evolution of oligomer size distributions. β-Strand propensity per residue. Dimer−dimer pairs, hexamer−hexamer pairs, and dimer−hexamer pairs. Tertiary and quaternary structures of Aβ oligomers. This material is available free of charge via the Internet at http://pubs.acs.org.

JA9096303